Optimal Scheduling Methods of Multi-Energy Systems

by

Jie Mei

B.S., Georgia Institute of Technology (2015)
S.M., Massachusetts Institute of Technology (2018)

Submitted to the Department of Electrical Engineering and Computer Science
in partial fulfillment of the requirements for the degree of

Doctor of Philosophy in Electrical Engineering and Computer Science

at the

MASSACHUSETTS INSTITUTE OF TECHNOLOGY

September 2021

Author……
Department of Electrical Engineering and Computer Science
August 25, 2021

Certified by……
James L. Kirtley
Professor of Electrical Engineering and Computer Science
Thesis Supervisor

Accepted by……
Leslie A. Kolodziejski
Professor of Electrical Engineering and Computer Science
Chair, Department Committee on Graduate Students

Optimal Scheduling Methods of Multi-Energy Systems

by

Jie Mei

Submitted to the Department of Electrical Engineering and Computer Science
on August 25, 2021, in partial fulfillment of the
requirements for the degree of
Doctor of Philosophy in Electrical Engineering and Computer Science

Abstract

In response to the challenge of improving energy production and consumption efficiencies due to environmental problems and energy crisis, multi-energy systems composed of electrical power, natural gas, heating power, cooling power networks and energy storage are attracting more attention and are being developed rapidly in recent years. Traditionally, different energy infrastructures are scheduled and operated independently, which results in less efficient energy usage and resource wasting. Through integrating as a multi-energy system, different energy carriers can be coupled and optimized as one unit to improve overall energy utilization efficiency, reduce system operating cost, and improving solar power integration.

In this thesis, optimal scheduling methods based on machine learning and optimization techniques of a real multi-energy system, Stone Edge Farm, CA, are proposed from an economic point of view. Specifically, Random Forest forecasting model is applied and further improved with online adaptability feature to provide input for the subsequent optimization. Besides, a new two-stage optimization formulation is proposed, which help greatly reduce computation time comparing with traditional integrated methods in the literature. Thus, the scheduling of MES operation can be conducted in much shorter time interval while considering more possible future scenarios.

Simulation results suggest that the proposed scheduling methods can help quantify the daily operating cost, balance real-time power demands and PV output solar power, and achieve considerable operating cost savings by appropriately arranging and utilizing all the devices in the multi-energy system.

Thesis Supervisor: James L. Kirtley
Title: Professor of Electrical Engineering and Computer Science

Acknowledgments

First and foremost my sincere thanks to my thesis supervisor, Professor Kirtley, who brought me into the door of scientific research and guided me from many different perspectives. His patience and support have been tremendously helpful throughout my entire time at MIT. He gave me the freedom to do research, and I am grateful to have him as my advisor. I think that what I have learned from him is not limited to scientific research, but all aspects of life. Time flies too fast, six years passed in a blink of an eye. I still remember when I was a senior at Georgia Tech, I emailed Professor Kirtley to ask about Ph.D. study at MIT. Professor Kirtley answered my questions quickly and in detail, which made me full of confidence in my application.

I would also like to thank my committee members, Professors Lang and Peng, for their helpful guidance on how to improve my work. Professor Lang, who has always been patient and humble, also gave me the opportunity to serve as a teaching assistant in the class he taught. I have learned a lot from these teaching and lab experiences, and I am grateful to have the opportunity to learn from him. Professor Peng was a visiting scholar at MIT and now works at the National University of Singapore (NUS). Thank you for your willingness to join the committee during your busy schedule and for providing valuable suggestions. Your keen insight into the energy systems has given me a lot of inspiration.

I want to thank my academic advisor, Professor Leeb. During my years of studying at MIT, Professor Leeb has given me a lot of advice on course selection and graduation. Professor Leeb is very approachable and always creates a relaxed atmosphere. I also especially thank Professor Leeb for his help and advice in RQE.

I express gratitude to my office-mates Chris Lee, Mathew Overlin and Xuntuo Wang (Nelson). I learned a lot from them. In particular, Chris was a huge help in our Magna motor design project. I appreciate this. I want to acknowledge Nelson for all of the hours he spent summarizing the system data of Stone Edge Farm. I would also like to thank the other members of Professor Kirtley's group, Mohammad Qasim, Krishan Kant, and Sajjad Mohammadi, and all the students and staff at LEES in general. I am thankful for all the staff at the EECS Headquarters. In particular, I wang to thank Janet Fisher, Kathleen McCoy, Alicia Duarte, and Leslie Kolodziejski.

I am grateful for all the friends I made at MIT and Harvard in general. A special thanks to my great friends Hongge Chen, Guannan Qu, and Yuhao Wang, who have enriched my life. I would like to thank them all for making Boston feel like at home.

I want to thank my family in my hometown in Beijing. In particular, I want to thank my father Shengwei Mei and my grandma Fanqing Dan. They always supported me unreservedly when I was growing up. I also want to thank my wife Xinran Zang. We met each other in middle school, and she became my girlfriend almost at the same time I received my MIT admission. I am very grateful to her for her willingness to tolerate all my problems.

I would like to thank my project sponsors, Tommy Energy, and Mac McQuown, owner of Stone Edge Farm in Sonoma, CA. Thank you for all your support. I am deeply grateful.

I would like to thank Professor Na Li from Harvard University, Professor Lang Tong from Cornell University, Professor Felix Wu from UC Berkeley, Professor Jianhui Wang from Argonne National Laboratory, Professor Qiang Lu from Tsinghua University, Professor Ming Cao from University of Groningen, Professors Thomas Habetler, Ronald Harley and Sakis Meliopoulos from Georgia Tech. Thank you all for providing me various research internship opportunities and writing me recommendation letters during my undergraduate and graduate

studies.

Finally, I would like to thank MIT for admitting me and giving me 6 years to work with and learn from the most diligent and smartest people in the world.

Contents

List of Figures

List of Tables

NOMENCLATURE

Variables

D^{c}	Cooling power demand from load
D^{e}	Electric power demand from load
D^{h}	Heating power demand from load
D^{FCEV}	Hydrogen power demand from load
E^{BS}	Stored electric energy in BS
E^{HS}	Stored hydrogen energy in HS
$I^{BS,\,cha}$	Binary indicator of BS charging status
$I^{BS,\,dis}$	Binary indicator of BS discharging status
$I^{EHP,\,c}$	Binary indicator of EHP cooling status
$I^{EHP,\,h}$	Binary indicator of EHP heating status
$I^{HS,\,cha}$	Binary indicator of HS charging status
$I^{HS,\,dis}$	Binary indicator of HS discharging status
P^{AC}	Output cooling power from chiller
P^{B}	Output heating power from boiler
$P^{BS,\,cha}$	BS charging electric power
$P^{BS,\,dis}$	BS discharging electric power
P^{CHP}	Input natural gas power of CHP
$P^{CHP,\,e}$	Output electric power from CHP
$P^{CHP,\,h}$	Output heating power from CHP
$P^{Com,\,BS}$	Output electric power from common bus to BS

P^{EHP}	Input electric power of EHP
$P^{EHP,\ c}$	Output cooling power from EHP
$P^{EHP,\ h}$	Output heating power from EHP
$P^{HS,\ cha}$	HS charging electric power
$P^{HS,\ dis}$	HS discharging hydrogen power
P^{FCEV}	Direct converted hydrogen power for FCEVs
P^{PU}	Purchased electric power from power utility
P^{NG}	Purchased natural gas power
P^{PV}	Solar power from roof photovoltaic arrays
$P^{PV,\ max}$	Instant maximum available solar power
s	Scenario index
t	Time
ρ^{e}	Unit price of electric power per kWh
ρ^{g}	Unit price of gas price per therm

Parameters

B	Number of CART in RF
$D^{c\prime}$	Mean of cooling power demand
$D^{c,\ \sigma}$	Standard deviation of cooling power demand
$D^{e\prime}$	Mean of electric power demand
$D^{e,\ \sigma}$	Standard deviation of electric power demand
$D^{h\prime}$	Mean of heating power demand
$D^{h,\ \sigma}$	Standard deviation of heating power demand
$D^{FCEV\prime}$	Mean of hydrogen power demand
$D^{FCEV,\ \sigma}$	Standard deviation of hydrogen power demand
$E^{BS,\ initial}$	Initial stored electric energy in BS

$E^{BS,\,max}$	Maximum stored electric energy in BS
$E^{HS,\,initial}$	Initial stored hydrogen energy in HS
$E^{HS,\,max}$	Maximum stored hydrogen energy in HS
m	Number of candidates split variables at each split
n_{min}	Minimum node size
N	p-dimension samples along with their class labels
N_{HL}	Number of hidden layer of ANN
N_I	Number of neurons in the input layer of ANN
N_{L1}	Number of neurons in the first hidden layer of ANN
N_{L2}	Number of neurons in the second hidden layer of ANN
N_{L3}	Number of neurons in the third hidden layer of ANN
N_O	Number of neurons in the output layer of ANN
$P^{AC,\,max}$	Maximum output cooling power from chiller
$P^{B,\,max}$	Maximum output heating power from boiler
$P^{BS,\,cha,\,max}$	Maximum BS charging electric power
$P^{BS,\,dis,\,max}$	Maximum BS discharging electric power
$P^{CHP,\,e,\,max}$	Maximum output electric power from CHP
$P^{CHP,\,h,\,max}$	Maximum output heating power from CHP
$P^{EHP,\,c,\,max}$	Maximum output cooling power from EHP
$P^{EHP,\,h,\,max}$	Maximum output heating power from EHP
$P^{HS,\,cha,\,max}$	Maximum HS charging electric power
$P^{HS,\,dis,\,max}$	Maximum HS discharging hydrogen power
$P^{FCEV,\,max}$	Max direct converted hydrogen power in HS
$P^{PV,\,max,}$	Mean of maximum solar power
$P^{PV,\,max,\,\sigma}$	Standard deviation of maximum solar power
p	Order number of autoregressive models

q	Order number of moving average models
S	Total scenario number
T	MES scheduling horizon
T_I	Set of time on the hour
ΔT	Any time interval for scheduling
ΔT_R	Time interval for real-time scheduling
$\hat{Y}_b$	The prediction of the b_{th} CART
$\hat{Y}_{rf}^{B}$	The prediction of the RF
Z^*	Bootstrap sample
η^{AC}	Chiller gas-to-cooling efficiency
η^{B}	Boiler gas-to-heating efficiency
$\eta^{BS,\,cha}$	BS charging efficiency
$\eta^{BS,\,dis}$	BS discharging efficiency
$\eta^{CHP,\,e}$	Electric percentage of CHP output power
$\eta^{CHP,\,h}$	Heating percentage of CHP output power
$\eta^{EHP,\,c}$	EHP electric-to-cooling efficiency
$\eta^{EHP,\,h}$	EHP electric-to-heating efficiency
$\eta^{HS,\,cha}$	HS charging efficiency
$\eta^{HS,\,dis}$	HS discharging efficiency
η^{FCEV}	HS direct electric-to-hydrogen efficiency
η^{PV}	Efficiency of the inverters of PVs
α	Confidence level of the two-stage scheduling method
β	Risk aversion parameter
φ	Confidence interval of RF models
σ	The minimum number of samples in adaptive RF
ξ	The minimum gamin in adaptive RF

Abbreviations

ANN	Artificial neural network
ARMA	Autoregressive moving-average
BS	Battery storage system
CART	Classification and regression tree
CHP	Combined heat and power device
EHP	Electric heat pump system
FCEV	Fuel cell electric vehicles
HS	Hydrogen storage system
MAPE	Mean absolute percentage error
MES	Multi-Energy System
MILP	Mixed-integer linear programming
PV	Solar photovaltalic panel
RF	Random Forest

Chapter 1

Introduction

1.1. Motivation

In the recent year, due to the growing concerns about environmental problems and energy crises, more efficient scheduling and management of energy production and consumption has been encouraged. Researchers have developed the concept of “smart grid”, which is an electricity network adopting a variety of operation and energy measures including smart meters, smart appliances, renewable energy resources, and energy efficient resources, and enabling a two-way flow of electricity and data and. Because of these new power grid concepts, lots of studies have focused on electrical technical issues. In response to the challenge of improving energy production and consumption efficiency, multi-energy systems (MESs) composed of electrical power, natural gas, heating power, cooling power networks and energy storage are attracting more attention and are being developed rapidly [1,2]. The initial concept and structure of MES are presented in [3,4]. Traditionally, different energy infrastructures are scheduled and operated independently, which results in less efficient energy usage and resource wasting [5,6]. Through integrating as a MES, where multiple energy carriers can be

converted and stored, different energy systems can be coupled optimized as one unit to improve overall energy utilization efficiency while meeting various energy demands.

Countries around the world have set aggressive goals in developing MES in recent years. The Department of Energy in the United States has proposed an integrated energy system plan since 2001[7]. Denmark has tried to accommodate a high penetration of renewable energy by developing combined heat and power devices (CHP) and central heating [8]. In China, the government issued an action plan for the construction of an Energy Internet, where building MES is one of the key tasks [9].

Optimal scheduling of MES is an optimization problem which specifies, at each point in time, optimal purchases of the considered energy sources, their dispatch among power converters, and optimal operation of the storage devices in the system [10]. Different methods have been proposed to solve the optimal scheduling problem in recent years. Under the assumption that accurate forecasts for demands and renewables are available to MES operator, the scheduling problem is formulated as mixed-integer linear programming (MILP) problem in [11-17]. However, for such deterministic optimization approaches, uncertainty and the stochastic nature of these inputs have not been considered. When the demands and renewables are subject to uncertainty over the scheduling horizon, the problem lends itself to a stochastic optimization formulation. Uncertainty in demands has been considered in [18-20], which propose scenario-based stochastic optimization formulations. Operating strategies for short-term dispatch of MES considering the uncertainty from renewables are proposed in [21-23]. In [24-26], stochastic and robust optimization models are proposed to address the uncertainties of various system components. In [28-30], genetic-algorithm-based methods are proposed to solve the optimal power flow scheduling problem for MES considering non-linear system characteristics. Besides those methods, data-driven robust stochastic programming approaches have been proposed in [31-36].

A few more works have further explored the merits of demand response applications in the scheduling of MES [37–41].

Furthermore, advancements in hydrogen fuel cell technology have also attracted the interest of researchers in recent years. As the penetration of renewable energy into the grid is increasing, hydrogen production from electrolysis where electricity comes from renewable sources can provide a sustainable way for production of hydrogen [42]. Authors in [43-45] introduced the hydrogen as a crucial production for sustainable development and discussed various types of hydrogen production such as solar thermal, photovoltaic, photoelectrolysis and biophotolysis. Hydrogen production from water using solar energy via a two-step thermochemical cycle was studied in [46], which further improves the hydrogen production efficiency. MESs with hydrogen applications were studied in [47-50]; it is shown that due to storage capability of this energy vector, more flexibility on energy conversion inside the MES is provided, which in turn brings more freedom and economic benefits in system scheduling and operation.

There are four aspects of the previous work that can be further advanced:

1) The previous scheduling methods in the literature usually neglects the forecasting of demands and renewables. They generally assume the future demands and renewables are given at the beginning of the scheduling and then perform the optimization while not updating the forecasts throughout the remaining operation horizon. However, the further ahead we forecast, the corresponding errors for demands and renewables increase. The large deviation between forecasted and actual values would increase the system operating cost, especially for small-scale community-level MES. Thus, it is important to integrate the forecasting into the optimization and keep updating forecasting results when designing such scheduling methods.

2) When taking different possible future scenarios into consideration based on the forecasting, the previous methods, such as MILP-based or Genetic-Algorithm-

based methods, are lack of computation efficiency. When different possible future scenarios are taken into consideration, those methods would need much computation time and are not suitable to do short-time-interval optimization, such as at minute-level.

3) In the previous studies considering hydrogen power, fuel cell electric vehicle (FCEV) related applications, for example, FCEV charging station, have not been exhaustively studied. Given the fact that today's FCEVs are becoming more and more popular, it is increasingly necessary to take FCEV-related applications into consideration when studying the MES optimal scheduling problem.

4) Most of the previous methods have not applied the data from a real MES and corresponding parameters for simulation and analysis, therefore the real physical characteristics and constraints of the key devices in MES have not been fully investigated.

1.2. Contribution

This thesis studies the optimal scheduling of a MES with FCEV applications considering the uncertainties of solar power and demands. An efficient two-stage optimal scheduling method based on machine learning and optimization techniques to address the real-time forecast deviations of demands and renewables is proposed. Stone Edge Farm, in Sonoma, California, would be treated as the exemplar of the proposed methods and a source of real-world data. The contribution of this work is fourfold:

1) Random Forest forecasting model is applied and modified to provide input for the optimization. Besides, the scheduling method incorporates the latest forecasted information throughout the scheduling horizon, which helps correct the previous forecast deviations, better schedule the storages for the remaining horizon, and in turn further reduce the operating cost.

2) Based on its two-stage formulation, the scheduling method generates close operating cost with the integrated method but with less computation time. By doing this, the scheduling optimization of MES operation in much shorter time interval considering more possible future scenarios is achievable.

3) Besides battery storage system (BS) in traditional MES in the literature, hydrogen storage system (HS) and charging station for FCEV are also considered in this work. The presence of HS can further improve operational flexibility over scheduling horizon through charging and discharging process.

4) The proposed optimal scheduling method is analyzed and simulated based on real MES data, thus the real characteristics of MES devices have been fully investigated.

It is also noteworthy that the proposed method has consider the current main MES devices. By modifying the corresponding equations that describing the specific system connection, the proposed method can be generally applied to other MESs worldwide besides Stone Edge Farm in this work.

1.3. Thesis Structure

The rest of this thesis is organized as follows. Chapter 2 describes the capabilities and operation constraints of the primary devices in the Stone Edge Farm MES and the corresponding system power flow diagram. Chapter 3 introduces the forecasting of demand and solar power based on random forest model for Stone Edge Farm MES. The online adaptability function of random forest would also be described. Chapter 4 explains the overall optimal scheduling method considering based on forecasting and optimization. Steps on how to improve the integrated method to a two-stage formulation would be provided in detail. Simulation results that show the merits of the proposed method are presented in Chapter 5, and conclusions are drawn in Chapter 6.

Chapter 2

Stone Edge Farm MES

Besides its lush landscapes, expansive vineyards, and world-class wines, the 16-arce Stone Edge Farm in Sonoma, California, is also one of the world-class test beds for MES development. It is expected to demonstrate the variety of clean energy solutions that can be used to produce, consume, manage, and store energy intelligently to reduce operating cost and carbon emissions while enabling winery operations and meeting various power demands.

Fig. 2-1 shows the Birdseye View of Stone Edge Farm MES. The corresponding power flow diagram is shown in Fig. 2-2. The Stone Edge Farm MES uses a complex fiber optic network that provides real-time monitoring and controlling remotely of each device of the MES via the farm's internet connection.

Section 2.1 introduces the functions and capabilities of the main devices in the Stone Edge Farm MES in detail where all the device parameters are listed in corresponding tables and figures of the devices are shown. Then in Section 2.2, the power flows between the devices and corresponding power balance constraints and the constraints from the devices will be described in detail as well.

Figure 2-1: Birdseye View of Stone Edge Farm MES, where the numbers are the solar locations. Picture Sourced from Stone Edge Farm Website [51].

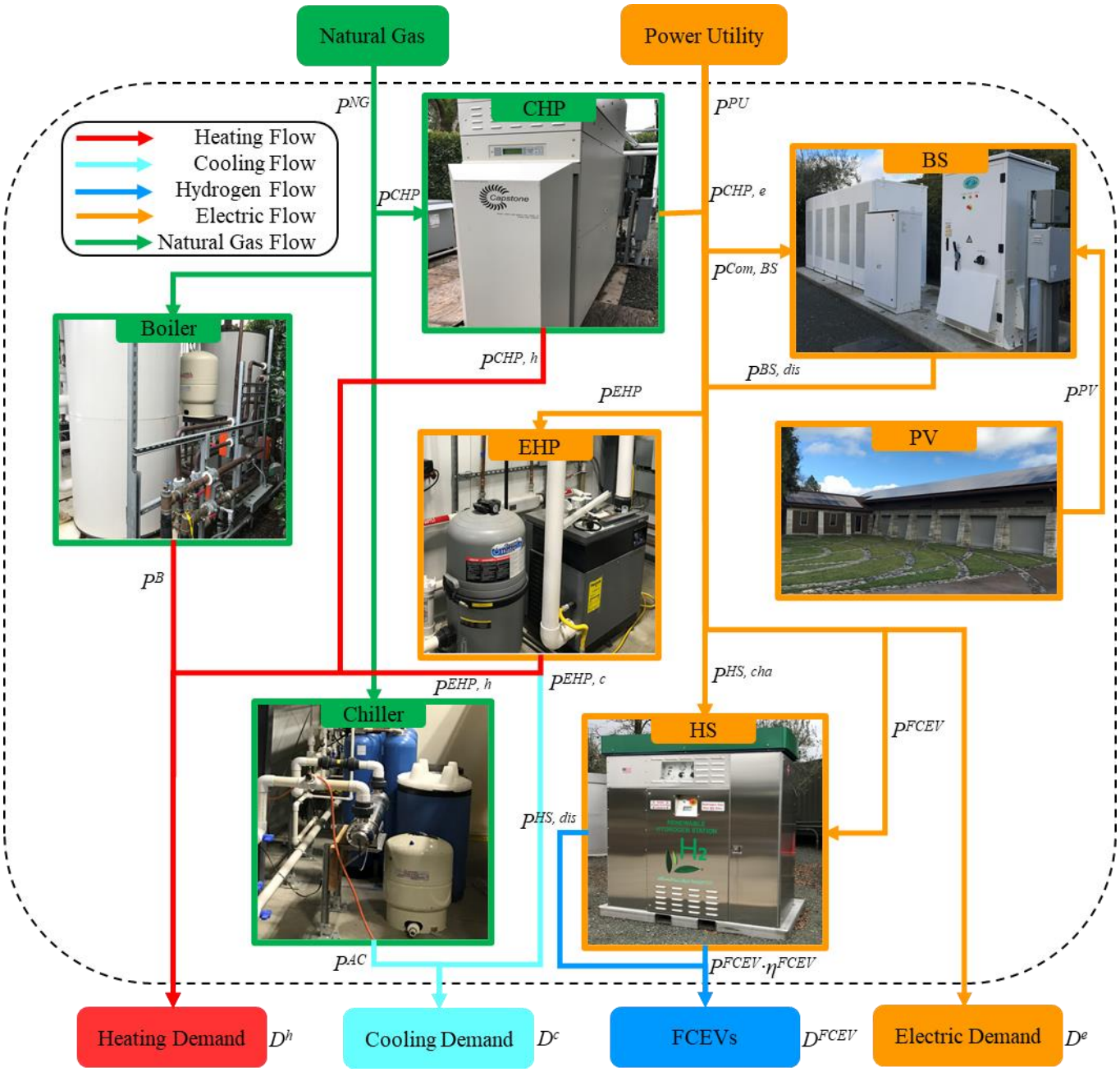

Figure 2-2: Power Flow Diagram of Stone Edge Farm MES.

2.1. System Devices

This section describes the primary devices of Stone Edge Farm MCESS and their functions. The main components of Stone Edge Farm MCESS include solar photovoltaic arrays (PVs), combined heat and power system (CHP), electric heat pump (EHP), absorption chiller, boiler, battery system (BS), hydrogen system (HS), and load, which will be illustrated in detailed throughout this section.

A. Solar Photovoltaic Arrays (PVs)

Electricity is supplied from the local power utility as well as onsite photovoltaic panels (PVs). Over 500 solar PVs are installed on the roofs of eight buildings around the property as shown in Fig. 2-3 with a maximum output power of 130kW, converted to AC by Enphase Energy M250 and S280 micro-inverters with an efficiency of 95% as in Table 2-1. The electric power injected to the MCESS from the solar photovoltaic arrays is less than the maximum available solar power at each time point. To maintain system reliability, solar power will be stored to BS directly.

Table 2-1: Parameters of PVs.

Parameter	Value
$P^{PV,\,max}$	130kW
η^{PV}	95%

Figure 2-3: PVs in Stone Edge Farm MES.

B. Combined Heat and Power Device (CHP)

The electric and heating systems are coupled by CHP in the Stone Edge Farm MES, which uses natural gas to produce electricity, and the waste heat from the Capstone turbine is a power generation source for balancing the heat loads in the heating system [52, 53]. CHP can meet heating and energy demand with less cost than EHP where local natural gas price is relatively lower than electricity price.

CHP in Stone Edge Farm MES is mainly driven by a Capstone Gas turbine C65 [54] natural gas-fired variable external combustion engine as shown in Fig. 2-4. Table 2-2 lists the parameters of the CHP. The combined heat and power efficiency is up to 90%. Among the converted power from natural gas, 68% goes to heating power and 22% becomes electric power. The Capstone Gas turbine uses natural gas to produce electricity, and waste heat from the turbine is a power generation source for a heater system. Considering CHP limitations, the

maximum output heating power is 52kW and maximum output electric power is 65kW, which would be the maximum available heating and electric power from CHP at different time point given certain amount of natural gas input. In some cases, much output electric power is needed while reaching the maximum output heating power limitation. In those cases, the part of output heating power beyond 52kW will be discarded due to the output heating power restriction.

Table 2-2: Parameters of CHP.

Parameter	Value
$P^{CHP,\,e,\,max}$	65kW
$P^{CHP,\,h,\,max}$	52kW
$\eta^{CHP,\,e}$	22%
$\eta^{CHP,\,h}$	68%

Figure 2-4: CHP in Stone Edge Farm MES.

C. Electric Heat Pump (EHP)

Another main energy conversion device in the MES is EHP, which can convert electric power into heating or cooling power. EHP system Jandy Pro Series Hi-E2 with water supply [55] as in Fig. 2-5 is used in the Stone Edge Farm MES. Table 2-3 lists the parameters of the EHP. The EHP system can generate a maximum heating power of 80kW or a maximum cooling power of 80kW. The corresponding efficiency of converting the received electric power to the output heating or cooling power is 95%.

Table 2-3: Parameters of EHP.

Parameter	Value
$P^{EHP,\,c,\,max}$	80kW
$P^{EHP,\,h,\,max}$	80kW
$\eta^{EHP,\,c}$	95%
$\eta^{EHP,\,h}$	95%

Figure 2-5: EHP in Stone Edge Farm MES.

D. Absorption Chiller

The absorption chiller is an add-on feature equipped on the CHP capstone turbine system as shown in Fig. 2-6. Table 2-4 lists the corresponding parameters. The maximum output cooling power is 65kW and the efficiency of converting the received natural gas to the output cooling power is 80%.

Table 2-4: Parameters of Absorption Chiller.

Parameter	Value
$P^{AC,\,max}$	65kW
η^{AC}	80%

Figure 2-6: Absorption Chiller in Stone Edge Farm MES.

E. Boiler

The boiler is also an add-on feature equipped on the CHP capstone turbine system in the Stone Edge Farm MES as shown in Fig. 2-7. Table 2-5 lists the corresponding parameters. The maximum output heating power is 80kW with an efficiency of 70% from converting the received natural gas.

Table 2-5: Parameters of Boiler.

Parameter	Value
$P^{B,\,max}$	80kW
η^{B}	70%

Figure 2-7: Boiler in Stone Edge Farm MES.

F. Battery System (BS)

The primary battery storage installed at the Stone Edge Farm is Tesla Lithium-Ion batteries rated at 250kW/475kWh [56] as shown in Fig. 2-8. This utility-scale

battery consists of five 50kW/95kWh cabinet-and-rack units, each containing 16 individual pods of lithium cobalt ion batteries. Table 2-6 lists the parameters of the BS. The charging efficiency is 92% with maximum charging power 250kW, and the discharging efficiency is 90% with maximum discharging power 250kW.

Table 2-6: Parameters of BS.

Parameter	Value
$E^{BS,\,max}$	475kWh
$P^{BS,\,cha,\,max}$	250kW
$P^{BS,\,dis,\,max}$	250kW
$\eta^{BS,\,cha}$	92%
$\eta^{BS,\,dis}$	90%

Figure 2-8: Tesla LithiumIon BS in Stone Edge Farm MES.

G. Hydrogen System (HS)

The HS at Stone Edge Farm consists of Millennium Reign Energy Series 3 hydrogen storage and fueling station SHFA model 300 as shown in Fig. 2-9 [57]. Hydrogen is generated from water with a hydrogen electrolyzer and further stored in 24 one-kg red carbon fiber and steel tanks to power Toyota Mirai FCEVs in the MES. Table 2-7 lists the parameters of the HS. The equivalent maximum HSS capacity is 800kWh.The maximum charging power is 400kW with efficiency of 80%, and the maximum discharging power is also 400kW with efficiency of 80%. A key function of the fueling station in HS is the direct FCEV charging by converting electric power with an efficiency of 80% and a limited capacity of 30kW instead of using the stored hydrogen energy in the tanks.

Table 2-7: Parameters of HS.

Parameter	Value
$E^{HS,\,max}$	800kWh
$P^{HS,\,cha,\,max}$	400kW
$P^{HS,\,dis,\,max}$	400kW
$P^{FCEV,\,max}$	30kW
$\eta^{HS,\,cha}$	80%
$\eta^{HS,\,dis}$	80%
η^{FCEV}	80%

Figure 2-9: Millennium Reign Energy Series 3 HS in Stone Edge Farm MES.

2.2. System Power Flow Constraints

2.2.1. Storage Constraints

A discrete-time model of power flow is developed in this work. Thus, the amount of energy in a storage system at the beginning of a certain time point is equal to the amount of energy at the previous time point considering the charged or discharged energies during that time period and the energy losses. Eq. (2.1) is used to model this storage transition function in the storage systems. The energy, which can be remained in each storage system, is bounded by the maximum energy capacities of the storage system as defined in Eq. (2.2).

$$E_{t+\Delta T}^{k} = E_{t}^{k} + P_{t}^{k,cha} \cdot \Delta T \cdot \eta^{k,cha} - \left(P_{t}^{k,dis} / \eta^{k,dis} \right) \cdot \Delta T, \quad \forall k \in \{BS, HS\} \quad (2.1)$$

$$0 \le E_{t}^{k} \le E^{k,max}, \quad \forall k \in \{BS, HS\} \quad (2.2)$$

2.2.2. Power Flow Capacity Constraints

Due to operation and safety considerations, devices cannot be operated above certain power levels. Eq. (2.3) and Eq. (2.4) refer to the maximum limits of the energy storage charging and discharging power, respectively. Since the energy storage cannot be charged or discharged at the same time, binary variables are adopted in this research to indicate the corresponding operation status and set the constraint at different time point as in Eq. (2.5).

$$0 \le P_{t}^{k,cha}(t) \le P^{k,cha,max} \cdot I_{t}^{k,cha}, \quad \forall k \in \{BS, HS\} \quad (2.3)$$

$$0 \le P_{t}^{k,dis}(t) \le P^{k,dis,max} \cdot I_{t}^{k,dis}, \quad \forall k \in \{BS, HS\} \quad (2.4)$$

$$0 \le I_{t}^{k,cha} + I_{t}^{k,dis} \le 1, \quad \forall k \in \{BS, HS\} \quad (2.5)$$

Eq. (2.6) and Eq. (2.7) represent the range of heating and cooling power that the EHP system can generate, respectively, after converting the receiving electric power. Similarly, as the EHP system cannot generate both heating and cooling power at the same time, corresponding binary variables are introduced to indicate the operation status and set the constraint as in Eq. (2.8). Eq. (2.2) summarize the input electric power of EHP.

$$0 \le P_{t}^{EHP,h} \le P^{EHP,h,max} \cdot I_{t}^{EHP,h} \quad (2.6)$$

$$0 \le P_{t}^{EHP,c} \le P^{EHP,c,max} \cdot I_{t}^{EHP,c} \quad (2.7)$$

$$0 \le I_{t}^{EHP,h} + I_{t}^{EHP,c} \le 1 \quad (2.8)$$

$$P_t^{EHP,v} = P_t^{EHP} \cdot \eta^{EHP,v}, \forall v \in \{h, c\} \tag{2.9}$$

It should be mentioned that the output electric and heating power of the CHP system are dependent on each other according to the combined heat and power efficiency, and therefore cannot be generated separately. Based on its conversion efficiency, the input natural gas power will generate a fixed proportion of 28% electric power and 62% heating power (constituting a total combined heat and power efficiency of 90%). Adding the capacity limitations of the CHP system, the corresponding output power range is:

$$0 \le P_t^{CHP,v} \le min\left\{P_t^{CHP} \cdot \eta^{CHP,v}, P^{CHP,v,max}\right\}, \forall v \in \{h, e\} \tag{2.10}$$

Finally, the generated heating and cooling power from the boiler and absorption chiller, the electric power injected to the MES from the PVs, and the direct-converted hydrogen power from the HS for FCEVs are limited by their maximum capacity and availability as shown in Eq. (2.11). Because the maximum available solar power is also a variable rather than a fixed value, this constraint is made as a separate equation in Eq. (2.12).

$$0 \le P_t^j \le P^{j,max}, \quad \forall j \in \{AC, B, FCEV\} \tag{2.11}$$

$$0 \le P_t^{PV} \le P_t^{PV,max} \tag{2.12}$$

2.2.3. Power Balance Constraints

In a MES, the power coupling between power loads $\boldsymbol{D}$ and input power sources $\boldsymbol{P}$ can be formulated linearly using coupling matrix $\boldsymbol{C}$ as Eq. (2.13):

$$\boldsymbol{D} = \boldsymbol{CP} \tag{2.13}$$

Specifically, for a MES with M types of power loads and N types of input power sources, Eq. (2.13) can be rewritten as Eq. (2.14):

$$\begin{bmatrix} D_1 \\ D_2 \\ \vdots \\ D_m \end{bmatrix} = \begin{bmatrix} c_{11} & c_{12} & \cdots & c_{1n} \\ c_{21} & c_{22} & \cdots & c_{2n} \\ \vdots & \vdots & \ddots & \vdots \\ c_{m1} & c_{m2} & \cdots & c_{mn} \end{bmatrix} \begin{bmatrix} P_1 \\ P_2 \\ \vdots \\ P_n \end{bmatrix} \tag{2.14}$$

where P_n and D_m denote the n-th type of input power source and the m-th type of power load, respectively; Coefficient c_{mn} denotes the corresponding coupling factor. The coupling factor is a combination of the dispatch and efficiency factors, where the efficiency is determined by the characteristics of the energy converter devices. The dispatch factor represents the operating status of the MES.

Through the power balance equations, MES power flows can be described. On the MES input side, the purchased natural gas is supplied to the CHP, boiler, and absorption chiller as in Eq. (2.15).

$$P_t^{NG} = P_t^B / \eta^B + P_t^{AC} / \eta^{AC} + P_t^{CHP} \tag{2.15}$$

For heating power balance, the demand is satisfied by the boiler, CHP, and EHP as shown in Eq. (2.16).

$$D_t^h = P_t^B + P_t^{CHP,h} + P_t^{EHP,h} \tag{2.16}$$

Cooling power demand is balanced through the chiller and EHP as in Eq. (2.17).

$$D_t^c = P_t^{AC} + P_t^{EHP,c} \tag{2.17}$$

The hydrogen power demand of FCEVs is supplied by the HS discharging power and the direct-converting function in HS as follows:

$$D_t^{FCEV} = P_t^{HS,dis} + P_t^{FCEV} \cdot \eta^{FCEV} \tag{2.18}$$

Eq. (2.19) summarizes the balance of electric power, where the input side includes the power bought from the local distribution power utility, the CHP, and BS discharging, and the output side includes the supplies to the BS charging, HS charging, the EHP, FCEV directly charging and the demand.

$$D_t^e + P_t^{EHP} + P_t^{FCEV} + P_t^{Com,BS} + P_t^{HS,cha} = P_t^{CHP,e} + P_t^{PU} + P_t^{BS,dis} \tag{2.19}$$

Finally, within the MES, besides the electric power input from the common bus, electric power from the PVs can also be used to charge the BS as formulated in Eq. (2.20).

$$P_t^{BS,cha} = P_t^{Com,BS} + P_t^{PV} \tag{2.20}$$

As a summary, this chapter describes the main devices and constraints of Stone Edge Farm MES. Unlike other existing MESs in the literature, Stone Edge Farm has its own hydrogen storage. Our subsequent forecasting and optimization parts will be based on the data of Stone Edge Farm. It should be also noted that we have not considered the startup and cooldown times of the devices in MES, which will be treated as one of the future works.

Chapter 3

Forecasting Based on Random Forest

The MES scheduling methods in the previous literature usually ignores the forecast of demand and renewable energy. They usually assume that future demand and renewable energy are given at the beginning of the scheduling, and then perform optimization without updating the forecast throughout the remaining operating horizon. However, it is well known that the further ahead the demands and renewables are forecasted, the corresponding errors increase. The large deviation between the predicted value and the actual value at the later part of scheduling will increase the operating cost of the system. Therefore, it is important to integrate forecasting into optimization when designing this scheduling method.

When demands and solar power are subject to uncertainty over the scheduling horizon, the MES optimal scheduling problem lends itself to a stochastic optimization formulation. In other words, the MES operator would need to forecast the values of demands and solar power throughout the scheduling horizon of the operation. The forecasting in this work is implemented by Random Forest (RF) models [58]. The main reason for selecting Random Forest is that it can provide a forecasting result distribution. This allows users to consider a variety of

scenarios that may occur in the future for optimization. Other models, such like artificial neural network (ANN), could not provide this feature.

In this chapter, introduction to RF will be given in Section 3.1. Then the forecasting result distribution and a revised online updating capability of RF will be explained in Section 3.2. Finally, the tuned RF models along with some benchmark models would be introduced in Section 3.3.

3.1. Introduction to Random Forest

RF is an ensemble learning method for classification and forecasting. It is based on two techniques, Classification and Regression Tree (CART) and Bagging. The CART, which is a tree-structured classification model that maps observations about an item to conclusions about the item's class [59], was first proposed by L. Breman in 1984 [60]. CART's advantage is that it can be fitted into data perfectly well. However, when conducting prediction or classification, CART suffers from high variance [61], because it can easily change as small change in input variable.

To solve this problem, CART was extended to RF through the other essential technique, Bagging, which generates new training sets by sampling from the original training data set uniformly and with replacement and was introduced by Breiman later in 1996 [62]. The introduction of Bagging will reduce the variance of CART while keeping the bias low. Moreover, RF adopts a trick called randomized node optimization to further reduce the CART variance. All above modifications to CART made by RF avoids the disadvantages of CART and proves to achieve nice forecasting accuracy.

Simple illustrations of CART and RF can be found in Fig. 3-1, where we can see that a CART decides in each node based on a split of a feature variable and makes its way down till reaching a leaf node [63]. In this simple illustration, there are 4 items (leaves) that are classified on the basis of two characteristics. A

decision concerning on characteristic is made at the upper node/row, and a decision concerning the second characteristic is made at the middle two nodes / middle row. Fig. 3-1 also provides a hint to the CART growing procedure: iteratively splitting each node into 2 sub-nodes by finding a best split variable along with a best split value till reaching minimum node size.

More detailed constructing and predicting stages of RF are presented in Algorithm 1. In brief, the procedure is to construct a multitude of CARTs fitted to bootstrap sampled datasets resampled from the original training set (bagging) [64]. At each decision node of a CART, instead of searching for the best split variable among all k variables, RF limits the candidate selected features, to m randomly chosen features. This is the randomized node optimization we mentioned above as a trick to reduce the CART variance. The best feature and split-point among the m features will be picked up based on how the labeled forecasted values are split. Then the node would be split into two daughter nodes and so does the sampled dataset. Recursively repeating the steps for each decision node of the CART, until the minimum node size n_{min} is reached. For the simple illustration in Fig. 3-1, n_{min} is 2 and B is 10. At predicting stage, RF predicts through the mode of the predictions generated by the fitted CARTs.

The RF model is extensively used in various classification and forecasting applications, such as medical [65-68] economic [69-72], transportation [73-75], climate [76-78], and engineering [79-82]. The merits of RF are summarized below:

1) RFs require only 3 input parameters, number of CARTs, minimum decision node size, and number of candidates split variables at each split.

2) RF can generate variable importance indices in its growing procedure, and they turn out to be nice estimates of variable relevancies.

3) RF is robust against irrelevant features and outliers in training data.

4) Structured as a tree, RF is able to expand itself to fit more data by growing more branches. This leads to the RF online learning algorithm and has made RF a nice adaptive machine learning model [83].

5) The feature of forecasting result distribution can provide input for the optimization considering multiple possible scenarios in the future.

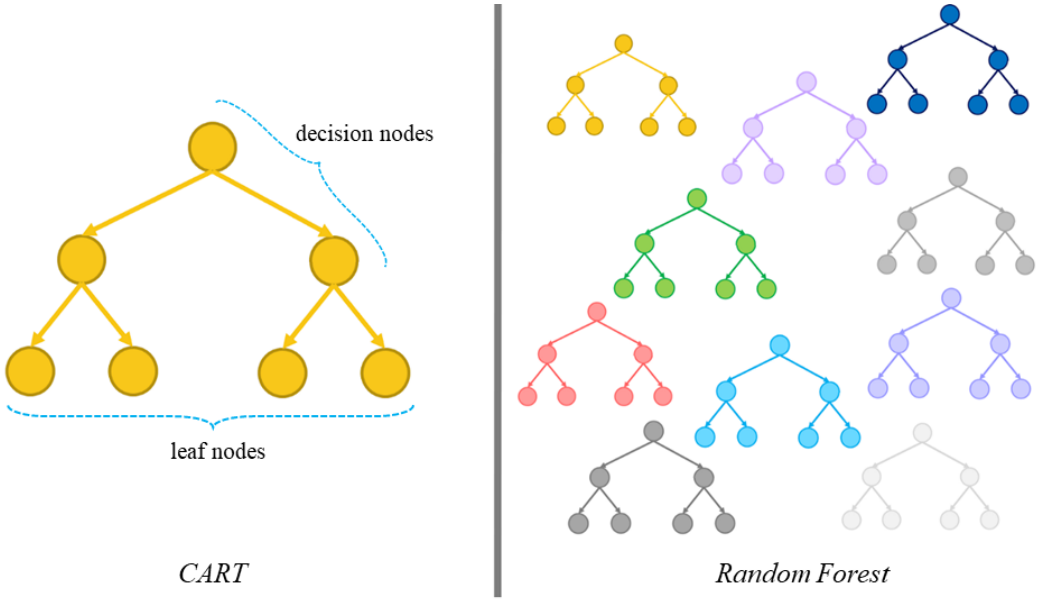

Figure 3-1: A Simple Illustration of CART and RF.

Algorithm 1. Growing and Prediction Stages of RF.

Growing Stage:

1. Input:
2. (a) Training Data *N*: *k*-dimension samples along with their class labels.
3. (b) Require Parameter *B*: Number of trees.
4. (c) Require Parameter *m*: Number of candidates split variables at each split;
5. (d) Require Parameter n_{min}: Minimum node size.
6. For b = 1 to B:
7. (a) Draw a bootstrap sample Z^* of size N from the training data.
8. (b) Grow a random-forest tree T_b to the bootstrapped data (generated data through bagging), by recursively repeating the following steps for each terminal node of the tree, until the minimum node size n_{min} is reached.
9. i. Select m variables at random from the p variables.
10. ii. Pick the best variable/split-point among the m.
11. iii. Split the node into two daughter nodes.
12. Output the ensemble of trees $\{T_b\}_1^B$:

Prediction Stage:

13. Let $\hat{Y}_b$ be the prediction of the bth random-forest tree. Then the output of RF can be generated as $\hat{Y}_{rf}^B = \frac{1}{B}\sum_{b=1}^{B}\hat{Y}_b$

3.2. Forecasting Result Distribution and Online Updating

As the anticipating process has some errors, the forecasting will not be completely accurate. Thus, it is necessary to model those uncertainties and take them into consideration when scheduling the MES operation, in which case different possible scenario cases and trade-off between operating cost and risk can be considered. The key feature, forecasting result distribution, provided by the RF would be discussed along with an added online updating function to make RF adaptable to new observed data and further improve its forecasting accuracy.

In the RF predicting procedure, the prediction is set as the mean of the predictions of the CARTs. Consider a set of observations *Y* and assume a CART *T* generates the classifications. Denote the posterior distribution of the CART parameters θ by $\theta|Y$. Consider *T* to be one of the trees in the RF model, then its parameters, $\hat{\theta}$, is estimated based on a bootstrap set sampled from *Y*. According to [84,85], such estimated parameters can be approximate the posterior distribution of the tree parameters $\theta|Y$. As such, the trees in the RF approximate the posterior distribution of the tree parameters $\theta|Y$. Therefore, the predictions of the trees, $\widehat{Y_b}(for\ b = 1 \dots B)$, reflect the posterior distribution of the prediction by the RF. They can be used to construct the forecasting result distribution attached to the prediction.

The next part of framework aims to update the random forest with new observations, so that the random forest can adjust to the latest forecasting condition. An online learning algorithm is introduced to update the random forest with a new observation, as shown in Algorithm 2. The key idea of the algorithm is summarized as follows:

In each tree, the new observation is processed repeatedly by γ times. This practice aims to simulate the bootstrap sampling procedure in the batch mode

random forest learning algorithm. The observation is processed as follows. Firstly, it is passed down from the root node to the leaf node which the observation belongs to. Then, a decision will be made on whether to split the leaf node into two child nodes or not. The decision is made based upon whether some leaf nodes receive enough new data that exceeds a predefined threshold and whether the possible reduce in training error is above the tolerance percentage value if the split was made [86].

Algorithm 2. Online Learning Capability of RF.

1. **Require**: Sequential training example: $< x, y >$
2. **Require**: The size of the forest: B
3. **Require**: The minimum number of samples: σ
4. **Require**: The minimum gain: ξ
5. // For all trees
6. **for** b from 1 to B **do**
7. $\gamma \leftarrow$ Poisson(λ)
8. // Update k times
9. **for** u from 1 to k **do**
10. j = findLeaf(x).
11. updateNode (j; $< x, y >$).
12. **if** $|R_j| > \alpha$ and $\exists s \in S$: $\Delta L\ (R_j, s) > \beta$ **then**
13. Find the best test: $s_j = \text{argmax}_{s \in S} \Delta L\ (R_j, s)$
14. createLeftChild(P_{jls})
15. createRightChild(P_{jrs})
16. UpdateGiniIndex.
17. **end if**
18. **end for**
19. **end for**
20. **Output** the forest.

3.3. Benchmark Forecasting Models for Optimal Scheduling

To show the merits of the RF with online learning function, the classic RF, ANN, and time-series autoregressive moving-average (ARMA) are treated as the benchmark models in this work. In this section, those forecasting models would be described in detail. We would explain their selected model parameters and forecasting features. Scheduling methods based on those different forecasting models would be compared later in the simulation chapter in terms of system operating cost.

A. Method 1: Classic RF

We define the classic RF model as our first forecasting method. The selected features for the prediction of each kind of demand after certain hours include:

- Demand at present, one hour ago, three hours ago, six hours ago, one day ago, one week ago, and one month ago
- Present and forecasted local temperature after certain hours
- Day indicator (Monday to Sunday)

The selected features for the prediction of the maximum available PV solar power after certain hours include:

- The maximum available PV solar power at present, one hour ago, three hours ago, six hours ago, one day ago, one week ago, and one month ago
- Present and forecasted temperature after certain hours
- Weather indicator (sunny, cloudy, showers, etc.) after certain hours

The features are selected because they are the available parameters collected during the experiment and based on the studies [87-91] that they are found to be the most impactful. The weather and temperature information are provided by

local weather forecast. The historical data from September 1st to November 10th, 2019, of Stone Edge Farm MES is treated as the training data set, and the data from November 11th to November 30th, 2019, is used as the test data set. Table 3-1 show the selected parameters of the classic RF based on experimentations (different combinations have been compared and the optimal values are chosen).

Table 3-1: Parameters of Classic RF.

Parameter	Value
B	500
m	3
n_{min}	5
φ	90%

B. Method 2: RF with online learning capability

We define the RF model with online learning capability as introduced in Algorithm 2 as the second forecasting method. The selected features, model parameters, and training data would be the same as forecasting method 1 except we selected the adaptability parameters introduced in Algorithm 2 based on experimentations as in Table 3-2:

Table 3-2: Parameters of Adaptive RF.

Parameter	Value
B	500
m	3
n_{min}	5
φ	90%
σ	10
ξ	0.1

As introduced earlier, a key feature provided by RF models would be the forecasting result distribution, which would be used in the proposed two-stage optimal scheduling method when dealing with operating cost and risk trade-off. As illustrations, Fig. 3-2 to Fig. 3-6 show the forecasted values of demands and maximum available PV output solar power for the next 24 hours starting at 8 am in an example winter day (Dec 17th, 2019) of Stone Edge Farm. The 90% confidence interval are also plotted in the same figures with lighter color. The accuracy of the forecasted mean values and the confidence interval are hourly based.

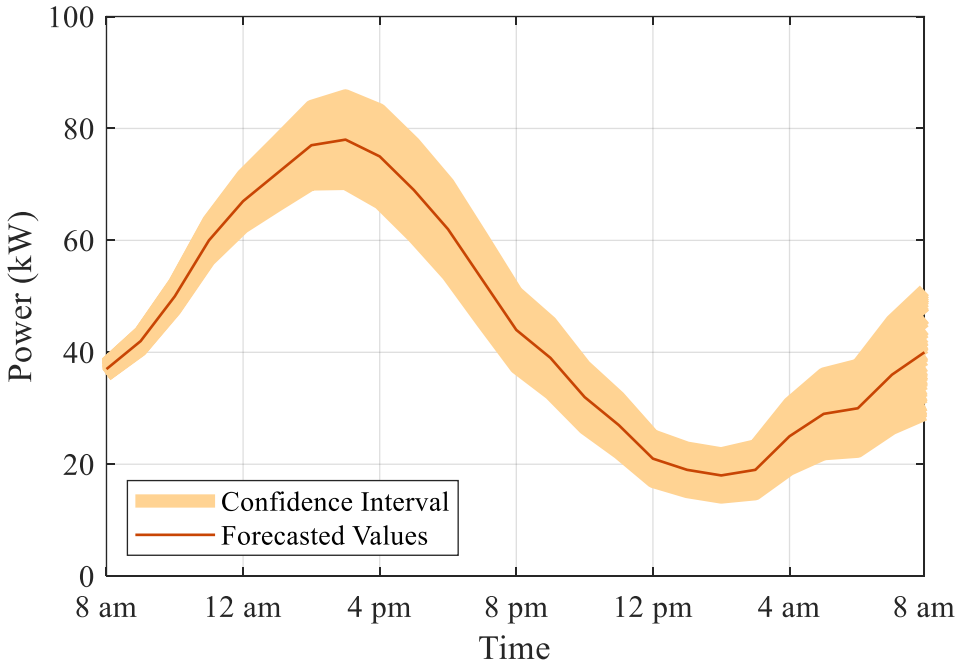

Figure 3-2: Forecasted Electric Power Demand for the Next 24 Hours.

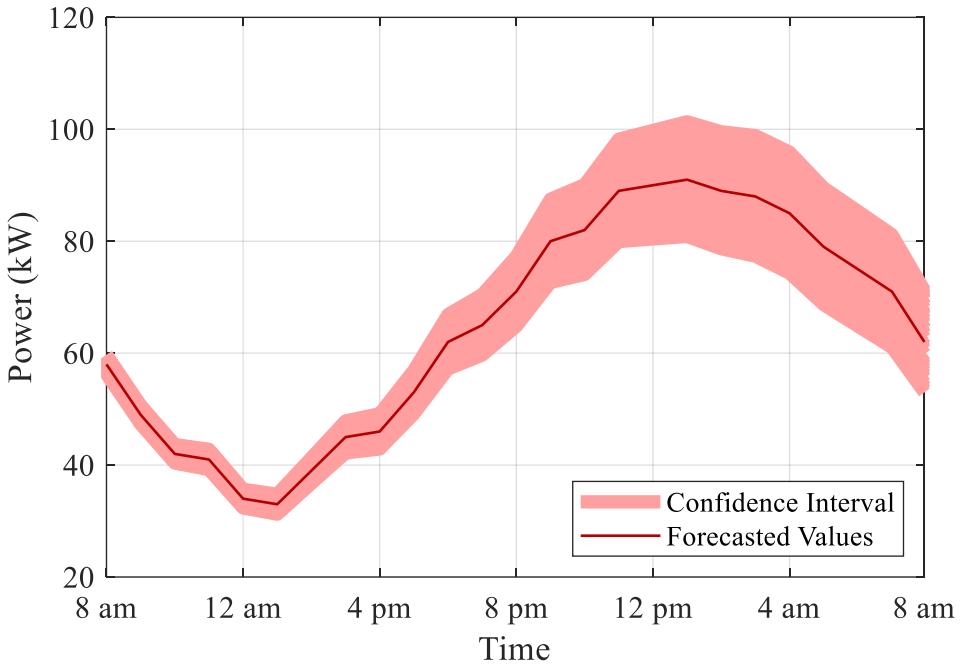

Figure 3-3: Forecasted Heating Power Demand for the Next 24 Hours.

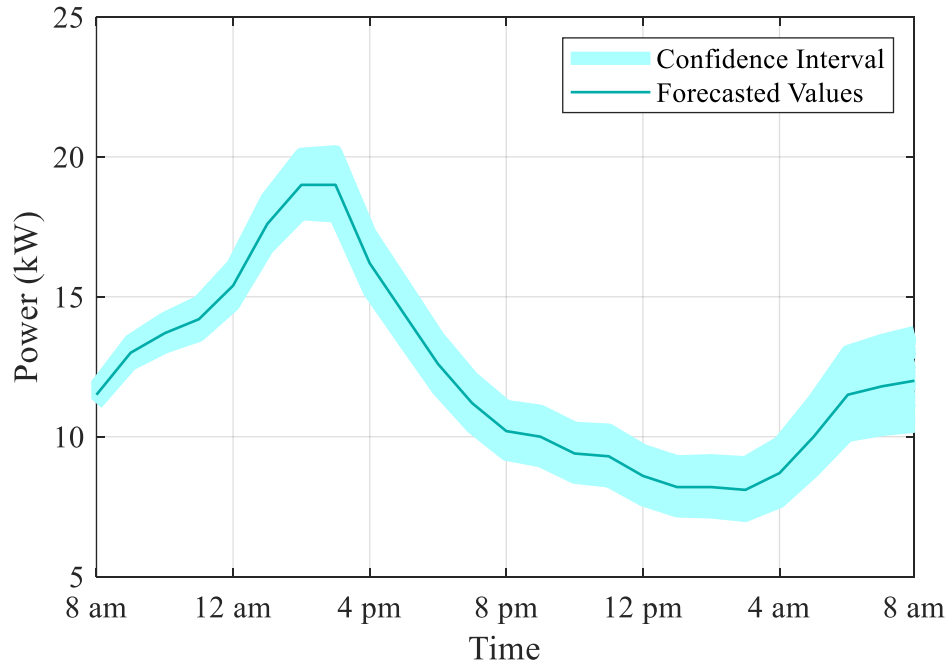

Figure 3-4: Forecasted Cooling Power Demand for the Next 24 Hours.

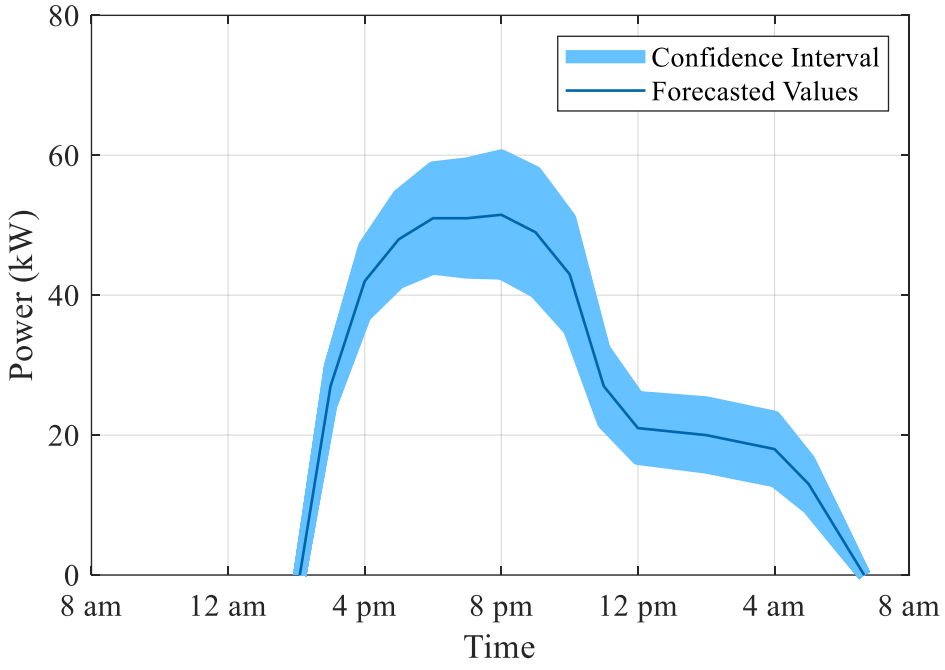

Figure 3-5: Forecasted Hydrogen Power Demand for the Next 24 Hours.

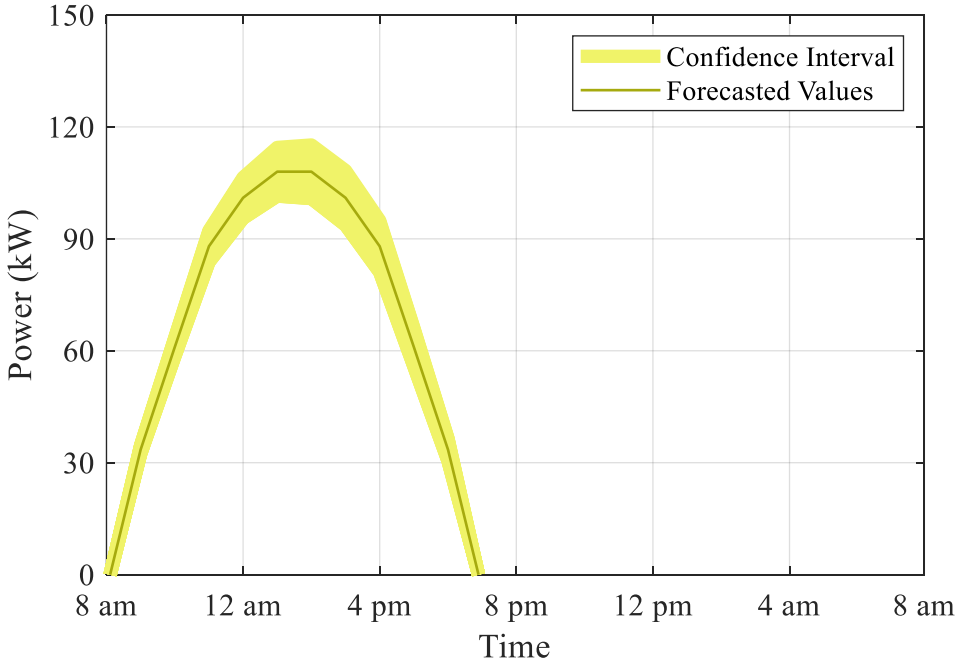

Figure 3-6: Forecasted Maximum Available Solar Power for the Next 24 Hours.

C. Method 3: ANN

An ANN is an interconnected group of nodes, akin to the vast network of neurons in a brain [92]. Typically, artificial neurons are aggregated into three different layers: input, hidden, and output, depending on their tasks [93]. Signals received from external inputs are first stored in the nodes in the input layer, and then processed to be transmitted to each of the nodes in the hidden layer [94]. These are finally transmitted to an output neuron in the output layer. ANNs have been proved to have the ability to learn sophisticated nonlinear relationships, which provides an ideal means of modelling complicated nonlinear forecasting and classification problems [95]. A simple illustration of ANN with one hidden layer of 5 neurons is shown in Fig. 3-7.

For the benchmark ANN in this work, the same features for RF models would be used. In more detailed, the selected features for the prediction of each kind of demand after certain hours include:

- Demand at present, one hour ago, three hours ago, six hours ago, one day ago, one week ago, and one month ago
- Present and forecasted local temperature after certain hours
- Day indicator (Monday to Sunday)

The selected features for the prediction of the maximum available PV solar power after certain hours include:

- The maximum available PV solar power at present, one hour ago, three hours ago, six hours ago, one day ago, one week ago, and one month ago
- Present and forecasted temperature
- Weather indicator (sunny, cloudy, showers, etc.) after certain hours

As there are 10 input features and 1 output forecasted value (demand or solar power certain hours later) for the ANN models, the input layer would have 10 neurons and the output layer would have 1 single neuron. Similarly, the historical data from September 1st to November 10th, 2019, of Stone Edge Farm MES is

treated as the training data set, and the data from November 11th to November 30th, 2019, is used as the test data set. Table 3-3 lists the parameters of the Benchmark ANN. Based on experiments, its optimal structure is tuned to be three hidden layers with 8 neurons in the first hidden layer, 6 in the second layer, and 4 in the third layer.

Table 3-3: Parameters of the Benchmark ANN.

Parameter	Value
N_I	10
N_O	1
N_{HL}	3
N_{L1}	8
N_{L2}	6
N_{L3}	4

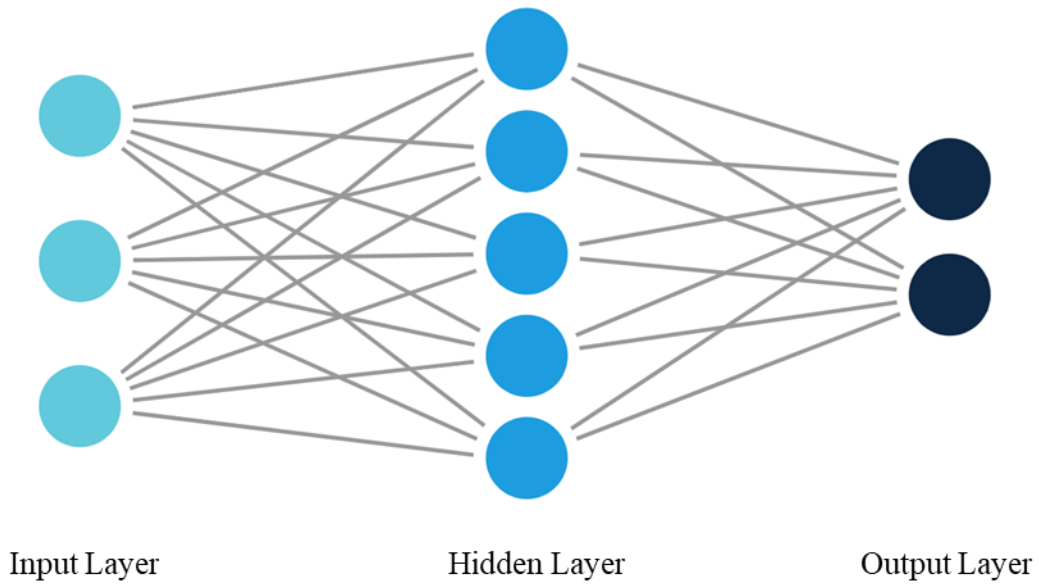

Figure 3-7: A Simple Illustration of ANN with One Hidden Layer.

D. Method 4: ARMA

In the statistical analysis of time series, autoregressive–moving-average (ARMA) models, developed by Peter Whittle in 1951, provide a parsimonious description of a stationary stochastic process in terms of two polynomials, one for the autoregression (AR) and the second for the moving average (MA) [96,97].

Given a time series of data, the ARMA model is a tool for predicting future values in this series. The AR part involves regressing the variable on its own lagged (i.e., past) values. The notation AR (p) refers to the autoregressive model of order p. The AR (p) model is written as Eq. (3.1) where $\varphi_1,\ldots,\varphi_p$ are parameters, c is a constant, and the random variable ε_t is white noise. The MA part involves modeling the error term as a linear combination of error terms occurring contemporaneously and at various times in the past. The notation MA (q) refers to the moving average model of order q, it can be written as Eq. (3.2) where the $\theta_1,...,\theta q$ are the parameters of the model, μ is the expectation of X_t, and the ε_t, $\varepsilon_{t-1},\ldots$are again, white noise error terms [93]. The notation ARMA (p, q) refers to the model with p autoregressive terms and q moving-average terms. Eq. (3.3) contains the AR (p) and MA (q) models. More introduction about ARMA models can be found in the literature [99-102].

$$X_t = c + \sum_{i=1}^{p} \varphi_i X_{t-i} + \varepsilon_t \tag{3.1}$$

$$X_t = \mu + \varepsilon_t + \sum_{i=1}^{q} \theta_i \varepsilon_{t-i} \tag{3.2}$$

$$X_t = c + \varepsilon_t + \sum_{i=1}^{p} \varphi_i X_{t-i} + \sum_{i=1}^{q} \theta_i \varepsilon_{t-i} \tag{3.3}$$

An ARMA (144, 30) model is proposed here where the parameters are also listed in Table 3-4. Because the ARMA model uses the same recent data to predict the future, previous 30 days demand and solar power historical data are

required to train the corresponding models.

The forecasting models are tested with the data of December, and the average mean absolute percentage errors (MAPEs) for the prediction of future demands and solar power after 1 and 24 hours are shown in Table 3-5 below. As can be seen from the results, the adaptive RF outperforms the benchmark models in terms of forecasting accuracy.

As summary, besides the fact that RF can provide a forecasting distribution feature such that more possible future scenarios can be considered in the optimization, its online learning feature is also expected to help lower operating cost comparing with the scheduling methods with other forecasting models. This is because whenever new observations are detected, the random forest can adjust to the latest forecasting condition. Thus, the forecasting accuracy can be improved.

Table 3-4: Parameters of ARMA.

Parameter	Value
p	144
q	30

Table 3-5: Comparison of different forecasting models.

Model	MAPE after 1 hour	MAPE after 24 hours
Adaptive RF	0.53%	4.36%
Classic RF	0.54%	4.81%
ANN	0.54%	4.84%
ARMA	0.82%	6.72%

Chapter 4

Optimal Scheduling Methods of Stone Edge Farm MES

In this chapter, we would study the optimal scheduling methods for Stone Edge Farm MES. Combining the forecasting from RF models, an integrated optimal scheduling method is introduced in Section 4.1. In Section 4.2, considering the computation efficiency issues, the integrated optimal scheduling method is improved to a two-stage structure and will be introduced in detail.

4.1. Integrated Optimal Scheduling Method

The purpose of stochastic optimization is to minimize the total expected operating cost of MES in the scheduling horizon, where the operating cost of MES in any time interval can be calculated by Eq. (4.1), which adds up the cost of purchased natural gas and electricity energy during that time interval.

$$C_t \overset{def}{=} \left(\rho_t^e \cdot P_t^{PU} + \rho_t^g \cdot P_t^{NG} \right) \cdot \Delta T \tag{4.1}$$

The system power flow variables at each moment are further defined as $\boldsymbol{X}_t$.

$$\boldsymbol{X}_t \overset{def}{=} \left(I_t^{BS,cha}, I_t^{BS,dis}, I_t^{EHP,c}, I_t^{EHP,h}, I_t^{HS,cha}, I_t^{HS,dis}, P_t^{AC}, P_t^{B}, P_t^{BS,cha}, P_t^{BS,dis}, P_t^{CHP} \right.$$
$$\left. P_t^{CHP,e}, P_t^{CHP,h}, P_t^{Com,BS}, P_t^{EHP}, P_t^{EHP,c}, P_t^{EHP,h}, P_t^{FCEV}, P_t^{PV}, P_t^{PU}, P_t^{HS,cha}, P_t^{HS,dis}, P_t^{NG} \right)$$

Following vectors are used to distinguish the actual and forecasted values.

$$\boldsymbol{U}_t \overset{def}{=} \left(D_t^c, D_t^e, D_t^h, D_t^r, P_t^{PV,max} \right)$$

$$\boldsymbol{U}_t' \overset{def}{=} \left(D_t^{c\prime}, D_t^{e\prime}, D_t^{h\prime}, D_t^{r\prime}, P_t^{PV,max\prime} \right)$$

The flow-diagram in Fig. 4-1 shows the integrated optimal scheduling method in actual Stone Edge Farm MES operation. In the first step, the demands and maximum available PV output of the entire scheduling horizon are forecasted based on RF models described in Chapter 3. In the second step, the optimal variables at each moment, which are all non-negative, are optimized for the entire operation horizon based on Eq. (4.2) and subject to constraints Eq (2.1) - (2.12), Eq. (2.15) – (2.20), and devices output limits as in Table 2-1 to 2-7. The scheduling method will be operated in a shrinking-horizon manner, in which the two steps will be repeated until the time reaches the operation horizon *T*.

$$\min_{\boldsymbol{x}_t} \sum_{t=0}^{T} C_t \left(\boldsymbol{X}_t, \boldsymbol{U}_t, \boldsymbol{U}_t' \right) \tag{4.2}$$

S.T.

$$E_{t+\Delta T}^k = E_t^k + P_t^{k,cha} \cdot \Delta T \cdot \eta^{k,cha} - \left(P_t^{k,dis} / \eta^{k,dis} \right) \cdot \Delta T, \quad \forall k \in \{BS, HS\} \tag{2.1}$$

$$0 \le E_t^k \le E^{k,max}, \quad \forall k \in \{BS, HS\} \tag{2.2}$$

$$0 \le P_t^{k,cha}(t) \le P^{k,cha,max} \cdot I_t^{k,cha}, \quad \forall k \in \{BS, HS\} \tag{2.3}$$

$$0 \le P_t^{k,dis}(t) \le P^{k,dis,max} \cdot I_t^{k,dis}, \quad \forall k \in \{BS, HS\} \tag{2.4}$$

$$0 \le I_t^{k,cha} + I_t^{k,dis} \le 1, \quad \forall k \in \{BS, HS\} \tag{2.5}$$

$$0 \le P_t^{EHP,h} \le P^{EHP,h,max} \cdot I_t^{EHP,h} \tag{2.6}$$

$$0 \le P_t^{EHP,c} \le P^{EHP,c,max} \cdot I_t^{EHP,c} \tag{2.7}$$

$$0 \le I_t^{EHP,h} + I_t^{EHP,c} \le 1 \tag{2.8}$$

$$P_t^{EHP,v} = P_t^{EHP} \cdot \eta^{EHP,v}, \forall v \in \{h, c\} \tag{2.9}$$

$$0 \le P_t^{CHP,v} \le min\{P_t^{CHP} \cdot \eta^{CHP,v}, P^{CHP,v,max}\}, \forall v \in \{h, e\} \tag{2.10}$$

$$0 \le P_t^{j} \le P^{j,max}, \quad \forall j \in \{AC, B, FCEV\} \tag{2.11}$$

$$0 \le P_t^{PV} \le P_t^{PV,max} \tag{2.12}$$

$$P_t^{NG} = P_t^{B} / \eta^{B} + P_t^{AC} / \eta^{AC} + P_t^{CHP} \tag{2.15}$$

$$D_t^{h} = P_t^{B} + P_t^{CHP,h} + P_t^{EHP,h} \tag{2.16}$$

$$D_t^{c} = P_t^{AC} + P_t^{EHP,c} \tag{2.17}$$

$$D_t^{FCEV} = P_t^{HS,dis} + P_t^{FCEV} \cdot \eta^{FCEV} \tag{2.18}$$

$$D_t^{e} + P_t^{EHP} + P_t^{FCEV} + P_t^{Com,BS} + P_t^{HS,cha} = P_t^{CHP,e} + P_t^{PU} + P_t^{BS,dis} \tag{2.19}$$

$$P_t^{BS,cha} = P_t^{Com,BS} + P_t^{PV} \tag{2.20}$$

The main problem for this integrated scheduling method is that all constraints will be applied at every time point of the entire scheduling horizon, determined by ΔT. Thus, when dealing with a shorter interval, such as minute-level power dispatch, it will suffer from heavy computation burden. For example, we may want to optimize in every 5 minutes in actual system operation, in other words, the time interval ΔT would be 5 mins, then the number of constraints would increase by a factor of 12 times comparing with the case when the time interval

ΔT is 60 mins. If the original number of constraints is 30, after the time interval is changed, this number would be 360. Besides, if more possible future scenario paths are considered when doing the optimization, we will have much heavier computation load. Due to the uncertainties from future demands and solar power, it is difficult to pre-calculate a look-up table off-line of the optimal system operation for all the possible future scenarios.

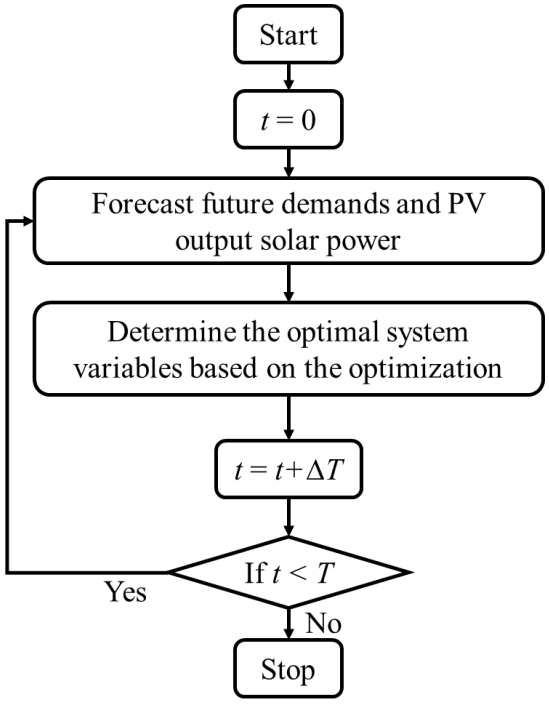

Figure 4-1: Flow-Diagram of the Integrated Optimal Scheduling Method.

Considering the two main design principle of the MES operation scheduling, one is to optimally store energy for future use, and the other is to balance real-time energy demand [103], we improve the integrated optimal scheduling method to a two-stage formulation as in the second section of this chapter so that it can generate close operating cost but with less computation burden and the computation time can be much shortened.

4.2. Two-Stage Optimal Scheduling Method

The flow-diagram in Fig. 4-2 shows the optimization process of the proposed two-stage optimal optimization method. The system power flow variables at each moment, which are all non-negative, are firstly divided into the storages charging- and discharging-related variables and others as $\boldsymbol{M}_t$ and $\boldsymbol{N}_t$.

$$\boldsymbol{M}_t \overset{def}{=} \left(I_t^{BS,cha}, I_t^{BS,dis}, I_t^{HS,cha}, I_t^{HS,dis}, P_t^{BS,cha}, P_t^{BS,dis}, P_t^{HS,cha}, P_t^{HS,dis} \right)$$

$$\boldsymbol{N}_t \overset{def}{=} \left(I_t^{EHP,c}, I_t^{EHP,h}, P_t^{AC}, P_t^{B}, P_t^{CHP}, P_t^{CHP,e}, P_t^{CHP,h}, P_t^{Com,BS}, P_t^{EHP} \right.$$
$$\left. P_t^{EHP,c}, P_t^{EHP,h}, P_t^{FCEV}, P_t^{PV}, P_t^{PU}, P_t^{NG} \right)$$

In the first-stage optimization, the hourly demands and maximum available PV output of the entire scheduling horizon are forecasted, and then the hourly optimal storage of energy for BS and HS is also calculated for the scheduling horizon based on Eq. (4.3) and subject to subject to constraints Eq (2.1) - (2.12), Eq. (2.15) – (2.20), and devices output limits as in Table 2-1 to 2-7. Based on reasonable charging and discharging scheduling for the storages according to the forecasted demands and PV solar power output, and energy price variations, the appropriate amount of energy with low cost can be stored, which can then be utilized to fulfill demands while achieving operating cost reduction.

The second term in Eq. (4.3) adds up the operating costs of the selected worst scenarios. In more detailed, *S* scenario paths are also generated in the first-stage optimization right after the forecasting. In each scenario path, for each hourly value to be forecasted, instead of outputting the average value of all the CARTs in RF, we output the forecasting result of a randomly selected CART. Scenario paths with high operating cost are always associated with high positive demand deviations and negative PV solar power deviations. Thus, the generated paths will

be evaluated according to these two indicators, and the worst $\alpha \cdot S$ scenarios, the ones with the most positive demand deviation and negative PV solar power deviation, will be selected as the worst possible future scenarios where α is a percentage number with the range of (0%, 100%). After adding the second term, the objective at this stage is to find the hourly optimal storage of energy for BS and HS for both the average future expectation and the worst expectations. By adjusting the weighting coefficient β, preference on costs of average future scenario and the worst scenarios can be emphasized.

$$\min_{\boldsymbol{M}_t,\boldsymbol{N}_t,\boldsymbol{N}_{t,s}} \sum_{t=0}^{T} C_t\left(\boldsymbol{M}_t,\boldsymbol{N}_t,\boldsymbol{U}_t,\boldsymbol{U}'_t\right) + \frac{\beta}{\alpha \cdot S} \sum_{s=1}^{\alpha \cdot S} \sum_{t=0}^{T} C_t\left(\boldsymbol{M}_t,\boldsymbol{N}_{t,s},\boldsymbol{U}_t,\boldsymbol{U}'_{t,s}\right) \tag{4.3}$$

S.T.

$$E_{t+\Delta T}^{k} = E_t^k + P_t^{k,cha} \cdot \Delta T \cdot \eta^{k,cha} - \left(P_t^{k,dis} / \eta^{k,dis}\right) \cdot \Delta T, \quad \forall k \in \{BS, HS\} \tag{2.1}$$

$$0 \le E_t^k \le E^{k,max}, \quad \forall k \in \{BS, HS\} \tag{2.2}$$

$$0 \le P_t^{k,cha}(t) \le P^{k,cha,max} \cdot I_t^{k,cha}, \quad \forall k \in \{BS, HS\} \tag{2.3}$$

$$0 \le P_t^{k,dis}(t) \le P^{k,dis,max} \cdot I_t^{k,dis}, \quad \forall k \in \{BS, HS\} \tag{2.4}$$

$$0 \le I_t^{k,cha} + I_t^{k,dis} \le 1, \quad \forall k \in \{BS, HS\} \tag{2.5}$$

$$0 \le P_t^{EHP,h} \le P^{EHP,h,max} \cdot I_t^{EHP,h} \tag{2.6}$$

$$0 \le P_t^{EHP,c} \le P^{EHP,c,max} \cdot I_t^{EHP,c} \tag{2.7}$$

$$0 \le I_t^{EHP,h} + I_t^{EHP,c} \le 1 \tag{2.8}$$

$$P_t^{EHP,v} = P_t^{EHP} \cdot \eta^{EHP,v}, \forall v \in \{h, c\} \tag{2.9}$$

$$0 \le P_t^{CHP,v} \le min\left\{P_t^{CHP} \cdot \eta^{CHP,v}, P^{CHP,v,max}\right\}, \forall v \in \{h, e\} \tag{2.10}$$

$$0 \le P_t^j \le P^{j,max}, \quad \forall j \in \{AC, B, FCEV\} \tag{2.11}$$

$$0 \le P_t^{PV} \le P_t^{PV,max} \tag{2.12}$$

$$P_t^{NG} = P_t^B / \eta^B + P_t^{AC} / \eta^{AC} + P_t^{CHP} \tag{2.15}$$

$$D_t^h = P_t^B + P_t^{CHP,h} + P_t^{EHP,h} \tag{2.16}$$

$$D_t^c = P_t^{AC} + P_t^{EHP,c} \tag{2.17}$$

$$D_t^{FCEV} = P_t^{HS,dis} + P_t^{FCEV} \cdot \eta^{FCEV} \tag{2.18}$$

$$D_t^e + P_t^{EHP} + P_t^{FCEV} + P_t^{Com,BS} + P_t^{HS,cha} = P_t^{CHP,e} + P_t^{PU} + P_t^{BS,dis} \tag{2.19}$$

$$P_t^{BS,cha} = P_t^{Com,BS} + P_t^{PV} \tag{2.20}$$

Because the real-time system operation is accompanied with uncertainties as described in the previous part, the second-stage optimization is designed for minute-level power balance as in Eq. (4.4), and subject to constraints Eq (2.6) - (2.12), Eq. (2.15) – (2.20), and devices output limits as in Table 2-1 to 2-5. In this stage, the storage charging and discharging variables in $\boldsymbol{M}_t$ calculated in the first stage are fixed for each hour, and only the power flow variables in $\boldsymbol{N}_t$ are optimized according to minute-level demands and PV output.

$$\min_{\boldsymbol{N}_t} C_t\left(\boldsymbol{M}_t, \boldsymbol{N}_t, \boldsymbol{U}_t\right) \tag{4.4}$$

S.T.

$$0 \le P_t^{EHP,h} \le P^{EHP,h,max} \cdot I_t^{EHP,h} \tag{2.6}$$

$$0 \le P_t^{EHP,c} \le P^{EHP,c,max} \cdot I_t^{EHP,c} \tag{2.7}$$

$$0 \le I_t^{EHP,h} + I_t^{EHP,c} \le 1 \tag{2.8}$$

$$P_t^{EHP,v} = P_t^{EHP} \cdot \eta^{EHP,v}, \forall v \in \{h, c\} \tag{2.9}$$

$$0 \le P_t^{CHP,v} \le min\left\{P_t^{CHP} \cdot \eta^{CHP,v}, P^{CHP,v,max}\right\}, \forall v \in \{h, e\} \tag{2.10}$$

$$0 \le P_t^{j} \le P^{j,max}, \quad \forall j \in \{AC, B, FCEV\} \tag{2.11}$$

$$0 \le P_t^{PV} \le P_t^{PV,max} \tag{2.12}$$

$$P_t^{NG} = P_t^{B} / \eta^{B} + P_t^{AC} / \eta^{AC} + P_t^{CHP} \tag{2.15}$$

$$D_t^{h} = P_t^{B} + P_t^{CHP,h} + P_t^{EHP,h} \tag{2.16}$$

$$D_t^{c} = P_t^{AC} + P_t^{EHP,c} \tag{2.17}$$

$$D_t^{FCEV} = P_t^{HS,dis} + P_t^{FCEV} \cdot \eta^{FCEV} \tag{2.18}$$

$$D_t^{e} + P_t^{EHP} + P_t^{FCEV} + P_t^{Com,BS} + P_t^{HS,cha} = P_t^{CHP,e} + P_t^{PU} + P_t^{BS,dis} \tag{2.19}$$

$$P_t^{BS,cha} = P_t^{Com,BS} + P_t^{PV} \tag{2.20}$$

The proposed two-stage scheduling method will also be operated in a shrinking-horizon manner, in which case it will repeatedly forecast the future demands and the maximum available PV output solar power, generate scenario paths, and run the first-stage optimization for the remaining scheduling horizon if the time is on the hour, and run the second-stage optimization every five minutes until the time reaches the end of scheduling horizon. Through this adaptability feature, the most recent forecasts about future demands and PV output solar power can be incorporated when conducting the optimal scheduling for the remaining operation horizon. Besides, due to its special structure, the computation burden is greatly reduced especially with short time interval, ΔT, and many scenario paths to be considered.

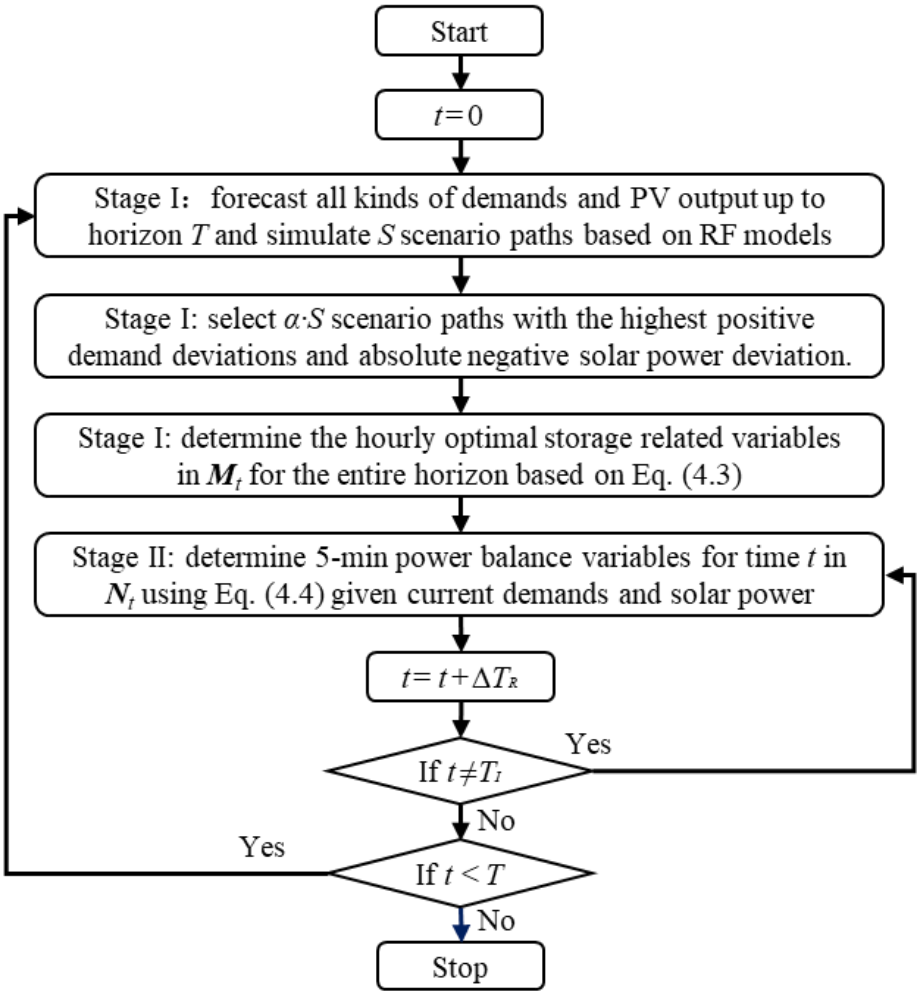

Figure 4-2: Flow-Diagram of the Two-Stage Optimal Scheduling Method.

As a summary, this chapter describes two scheduling methods that consist of forecasting and optimization. The integrated optimal scheduling method lacks computational efficiency, and it is difficult to apply in minute-level dispatch. The improved two-stage method can effectively help increase the computing speed. We will show more of this in the subsequent simulation chapter. Another thing to mention is that the optimization used in this chapter is MILP, which is not convex. The integer variables make the optimization not convex. Thus, we can only guarantee local minima.

Chapter 5

Simulation and Analysis

This simulation chapter is divided into six parts: in Case I, the optimal operation of Stone Edge Farm MES based on the proposed two-stage scheduling method is demonstrated for an example 24 hours, and the energy sources to meet the demands are analyzed in detailed. Case II analyzes the effects of PV and storage systems on reducing operating cost. In Case III, forecasting interval for future demands and PV output is changed and the corresponding effects on system operating cost are analyzed. In Case IV, the trade-off between operating cost and risk is studied. Case V explore the convergence of the proposed method, where the relations between the number of scenarios and the value of the objective function as well as the computation time are studied. Finally, in Case VI, the proposed method is compared with other typical MES operation scheduling methods in the literature in terms of operating cost and computation time to show its merits.

MATLAB R2019a is employed to handle the simulations in this chapter. In all the simulation Cases, the scheduling horizon T for the proposed method is set to 24 hours. Besides, all the simulations were run in an Intel Processor 5Y70 CPU 1.3 GHz environment.

5.1. Case I: MES Operation of An Example 24 Hours Based on the Proposed Method

In Case I, an example 24-hour period, from 8 am on Dec 17th to 8 am on Dec 18th, 2019, is selected to demonstrate detailly how the devices of Stone Edge Farm MES are optimally operated based on the proposed two-stage scheduling method. Besides the forecasted demands and maximum available PV output solar power for the next 24 hours starting at 8 am on Dec 17th as in Fig. 3-2 to Fig. 3-6, Fig. 5-1 shows the natural gas and electricity prices during the 24 hours. It can be shown from the figure that the local natural gas is much cheaper than electricity for getting the equivalent amount of energy after changing the unit of natural gas from therm to kWh (1 therm is approximately equals to 29.3 kWh).

After the proposed two-stage scheduling method is run for the 24-hour period with β and initial stored energy in BS and HS set to zero, detailed power flows and optimal scheduling for the MES are generated. The overall MES operating cost for this example 24-hour period is optimized to $417. If all future demand and solar power are given, that is, the optimal operating cost of the system will be $408.4. Thus, the difference between the result given by our method and the theoretical optimal value is about 2%, which is caused by the forecast errors.

In Fig. 5-2, the generated cooling power to meet the corresponding cooling power demand is plotted. It can be seen from the figure that the cooling power from the absorption chiller is preferred to that from the EHP because of the lower cost of local natural gas. For the example 24-hour period, cooling power demands are all met by the absorption chiller. Generally, only when the maximum cooling power generating capability of the chiller has been reached, the EHP will start to work in cooling status to help generate extra cooling power.

Similarly, as shown in Fig. 5-3, which plots the generated heating power to meet the heating power demand, the CHP is the priority when heating power is

needed. When the CHP output heating power reaches its limit with efficiency advantage, the boiler can generate the remaining required heating power to help meet the demand. Comparing with the CHP and boiler, the EHP would be the last choice for generating heating power because of the price advantage of local natural gas over electricity.

Fig. 5-4 shows the power sources for fulfilling load side electric power demand at different points in time. As shown in the figure, the CHP has the priority for supplying electric power. According to the characteristic of CHP, the combined heat and electric power efficiency, its electric power injected into the MES is maintained at about 16.8kW. Beyond this value, its efficiency advantage would no longer exist. Before 8 pm, because the battery is in charging status for most of the time, the remaining demanded electric power beyond 16.8kW will be purchased directly from the power utility. When the battery has been charged by the solar power, the remaining power demand is mainly supplied by the BS in the following time. Combined with the bought electric power from the local power utility and natural gas, and input solar power to the system, and the curves of 24-hour stored energy in the BS as in Fig. 5-6 and Fig. 5-7, it can be concluded that the most important role of BS in optimizing the scheduling is to store free solar power for future usage.

Finally, in Fig. 5-5, the generated hydrogen power to meet the hydrogen power demand for FCEVs is plotted. Combined with the MES input power in Fig. 5-6 and the 24-hour stored hydrogen power in the HS in Fig. 5-7, it can be seen that the majority hydrogen demand is supplied from the stored hydrogen in HS, which is charged mostly by the purchased electric power from the local power utility.

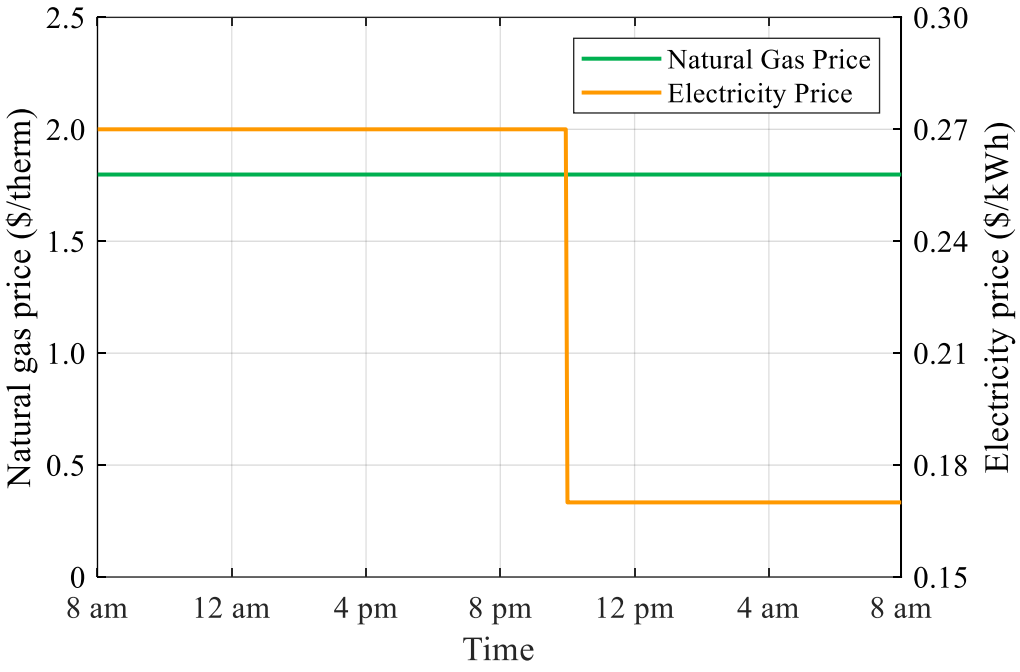

Figure 5-1: Electricity and Natural Gas Price for the Example 24 Hours.

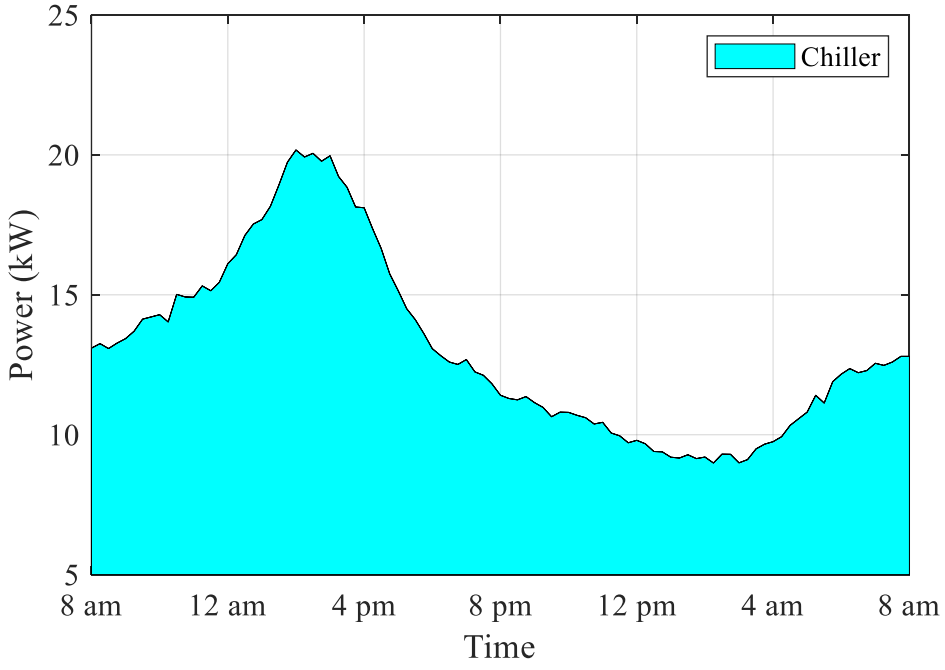

Figure 5-2: Cooling Power Demand and Sources for the Example 24 Hours.

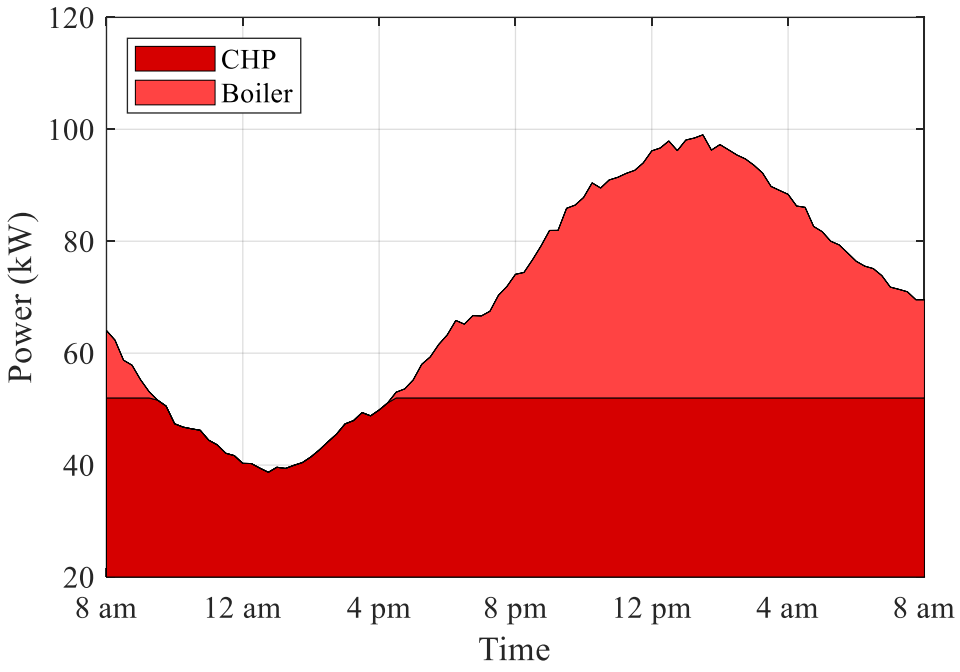

Figure 5-3: Heating Power Demand and Sources for the Example 24 Hours.

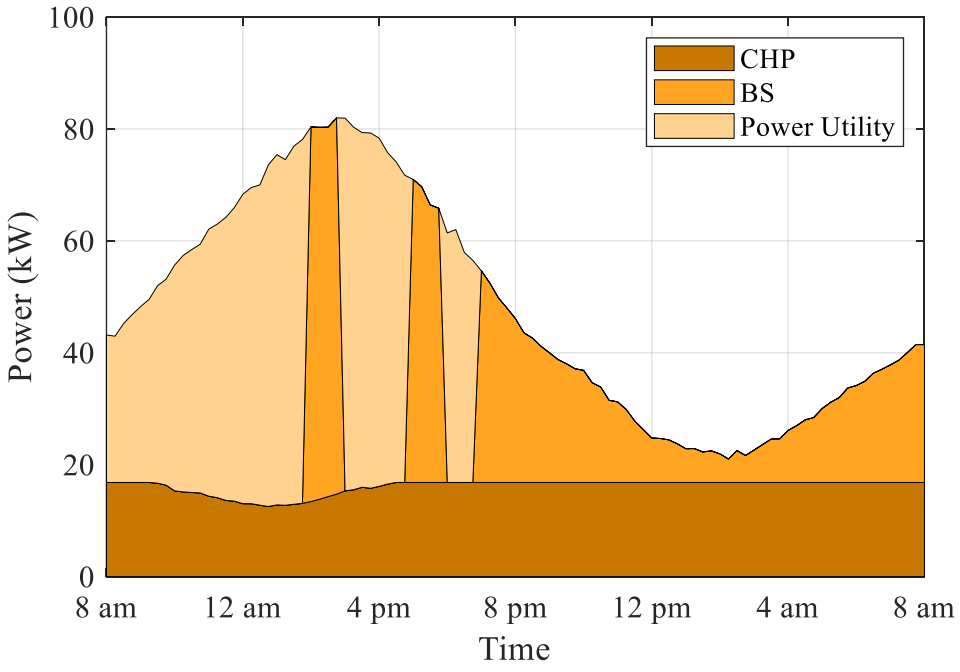

Figure 5-4: Electric Power Demand and Sources for the Example 24 Hours.

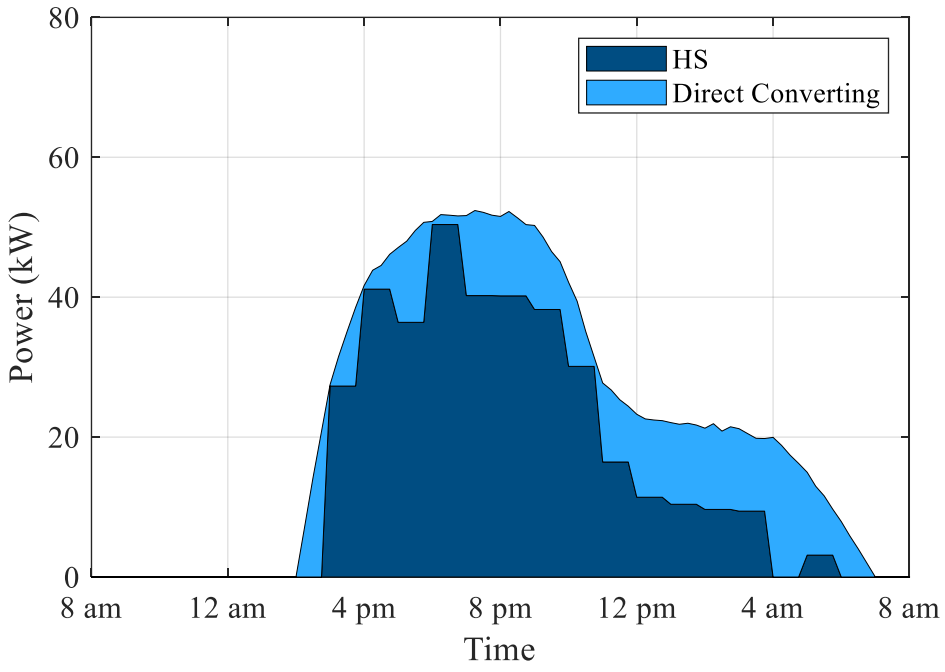

Figure 5-5: Hydrogen Power Demand and Sources for the Example 24 Hours.

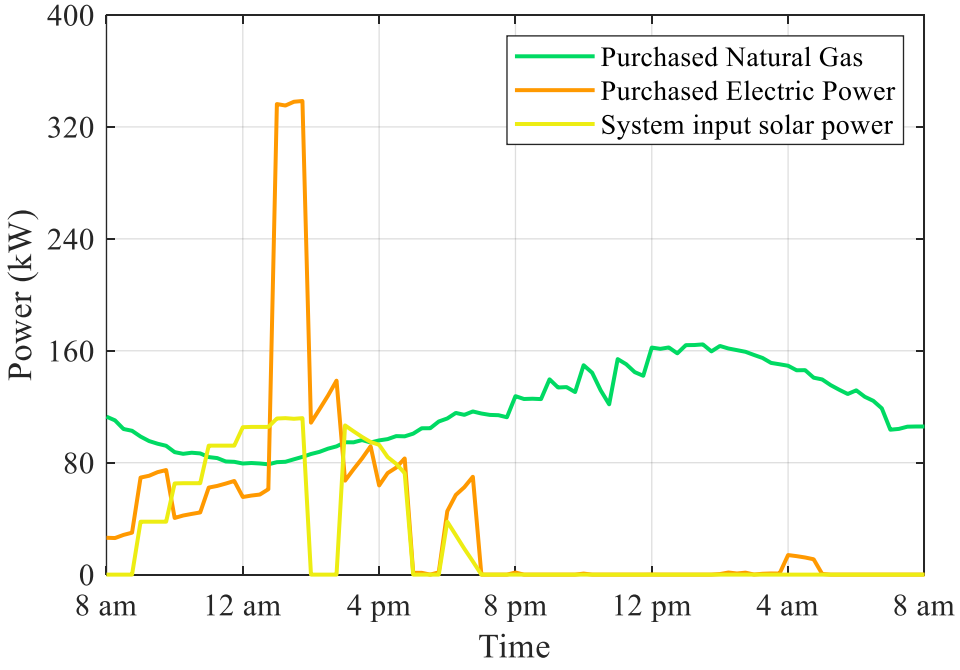

Figure 5-6: System Input Power for the Example 24 Hours.

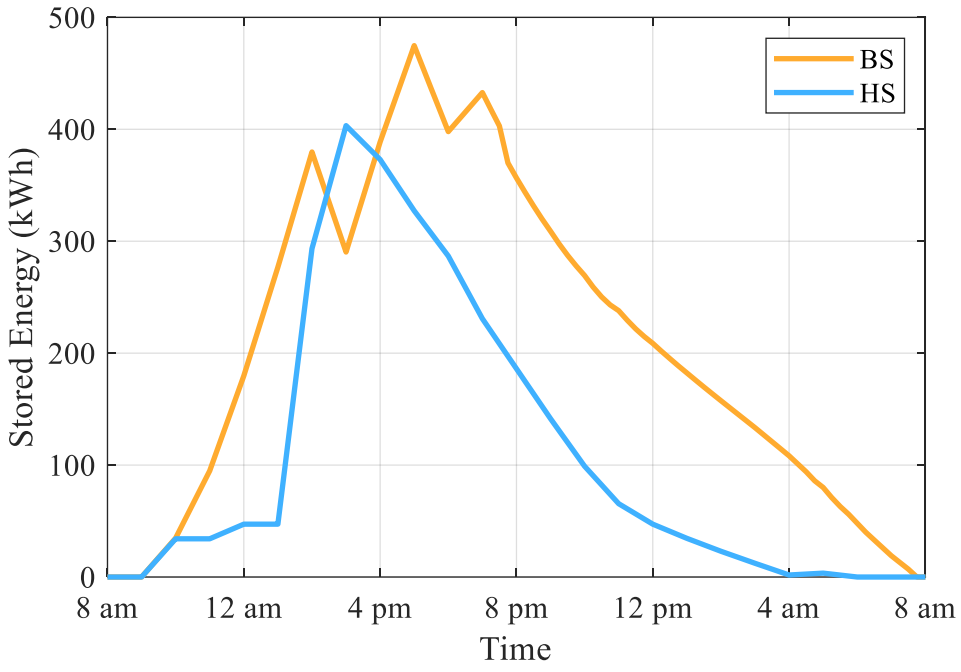

Figure 5-7: Stored Electric and Hydrogen Energies for the Example 24 Hours.

5.2. Case II: Effect of Storages and PVs on Operating Cost

In case II, the proposed method is applied to each day in December 2019 based on the recorded actual data to explore the effect of energy storages and PVs on reducing operating cost. Similarly, β and initial stored energy in BS and HS are set to 0, and during each 24-hour period from 8 am on every day to 8 am on next day the demands and solar power will be forecasted repeatedly in the first-stage optimization, but the actual values would be used for second-stage optimization. In Table 5-1, the operating costs with and without PVs and storage systems are listed to show their economic merits. With HS, BS, and PVs, the average daily operating cost is $415 for that month. If without HS, the average operating cost would be $434, suggesting a cost increase of 4.6%. It shows that installing HS

does not have much economic benefits especially considering the costly infrastructure upgrade. If without the PVs in the system, there will not be solar power and the system needs to purchase more electricity from local power utility to meet electrical demand. In this case, the cost would be increased to $535, equivalent to a cost increase of 29%. Finally, if there is no BS, the solar power will also not be able to store for future use as PVs is connected to BS directly in current setting and the system cannot use BS to coordinate energy usage. In this case, the cost would be $556, equivalent to a cost increase of 34%.

The results can show the benefits that the PVs and BS bring to the MES. With BS, solar power from the PVs can be utilized to the greatest extent. Moreover, based on reasonable charging and discharging scheduling for the BS according to the demands, solar power, and energy price, operating cost can be further reduced.

Table 5-1: Economic benefits of PVs and storages for MES.

	Cost ($)	Increase Percentage
Full System	415	N/A
Without HS	434	4.6%
Without PVs	535	29%
Without BS	556	34%

5.3. Case III: Effect of Forecasting Interval on Operating Cost

One of the major features of the proposed two-stage optimal scheduling method is that the energy storages in the MES will be planned hourly for the remaining scheduling horizon based on the latest forecasted future demands and PV output solar power as in our stage-I optimization. This is because the further ahead we forecast, the corresponding errors for demands and renewables increase.

Therefore, we need to constantly update the forecast results when scheduling.

Though this is a known fact, we still want to explore the benefits from short-interval forecasting. The simulation setting in Case II is maintained except the original forecasting interval is changed from one hour up to twelve hours, and the resulting average operating costs and increase percentages are shown in Fig. 5-8. It can be seen from the figure that as the forecasting interval increases, the operating cost of the system will also increase. When this interval is increased to 12 hours, that is, the first forecast is conducted at 8 am and the second one is at 8 pm, the average daily operating cost in December has also increased from the original $415 per day to $497 per day, equivalent to a 19.8% increase. As introduced earlier, the further ahead we forecast, the corresponding errors for demands and renewables increase. Therefore, by quickly and constantly incorporating the latest information of future demands and solar power, the previous forecasting deviations can be better corrected, and the storages can be better scheduled for the remaining horizon.

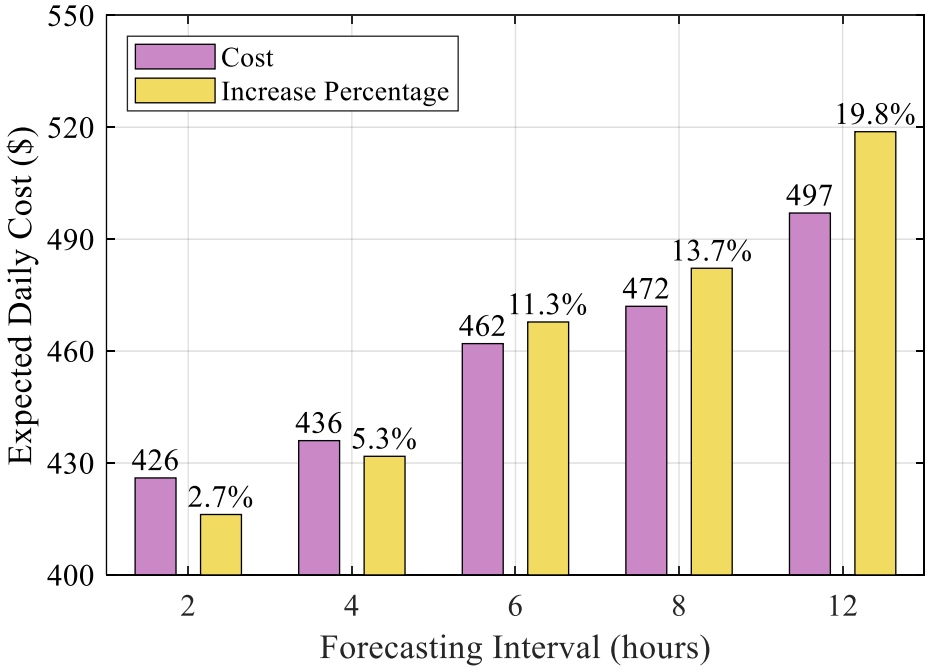

Figure 5-8: Operating Cost Comparison with Different Forecasting Intervals.

5.4. Case IV: Tradeoff between Operating Cost and Risk

In this Case, the effect of weighting parameter β of the cost of the worst possible scenarios is analyzed given the same simulation setting in Case II. The number of scenarios S is set to 100 and the confidence level α is set to 10%, which means the cost of the 10 worst scenarios are calculated and added up.

Fig. 5-9 depicts the expected average daily cost and aggregate cost of the worst cases with different β values. As shown in the figure, when $\beta = 0$, the average expected daily cost is \$415 while the aggregate cost of the 10 worst cases is \$4350. When $\beta = 1$, the expected daily cost increases to \$425 and the aggregate cost of the worst cases decreases to \$4265. It can be concluded that when the level of risk-aversion increases, the aggregate cost of the worst cases decreases and the expected daily cost increases. In another words, low levels of risk are associated with high costs, and vice versa. The main reason here is that by adjusting β value, the expectations of energy storage for future demands and solar power would be adjusted accordingly: taking a large β means storing more energy for possible big forecasting deviations in the future, then when such deviations happen, the system is already well-prepared, while a smaller β means focusing more on optimizing the mean forecasted values.

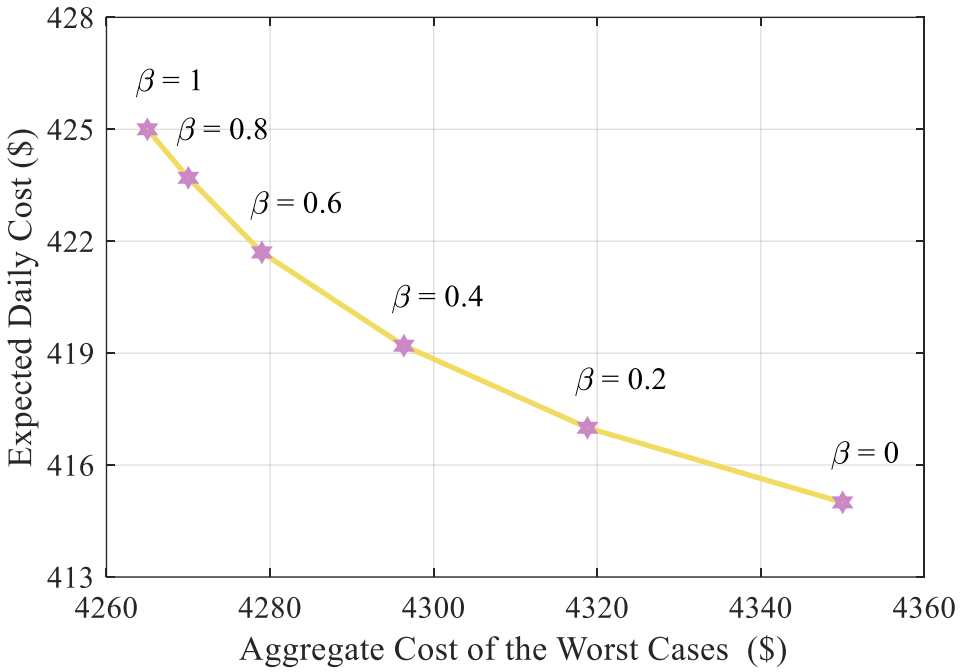

Figure 5-9: Trade-Off between Operating Cost and Risk.

5.5. Case V: Convergence Analysis

In Case V, the convergence of the proposed two-stage method is analyzed given the same simulation setting in Case II except with different β values and number of scenarios, and the confidence level α is set to 10%.

Fig 5-10 depicts the expected average daily cost of December for different number of scenarios with different β values. It can be seen from the figure that when the number of scenarios is above 200, continuingly increase the number of scenarios could not help significantly reduce the daily system operating cost.

On the other hand, Fig. 5-11 shows the expected average daily computation time of applying the proposed two-stage method with different number of

scenarios where β is set to 0.6. The computation time generally comes from the forecasting stage of RF and also the optimization. It can be seen from the figure that when the number of scenarios increases, the computation time also increases exponentially as heavier computational burdens are added at the same time. Comparing the relationship between the number of scenarios and the expected average daily cost, as well as the computation time, it would be more efficient to operate the Stone Edge Farm MES with the number of scenarios set below 200 when the risk of the worst possible scenarios as described in Case IV (α is set to 10%) is considered in daily system operation.

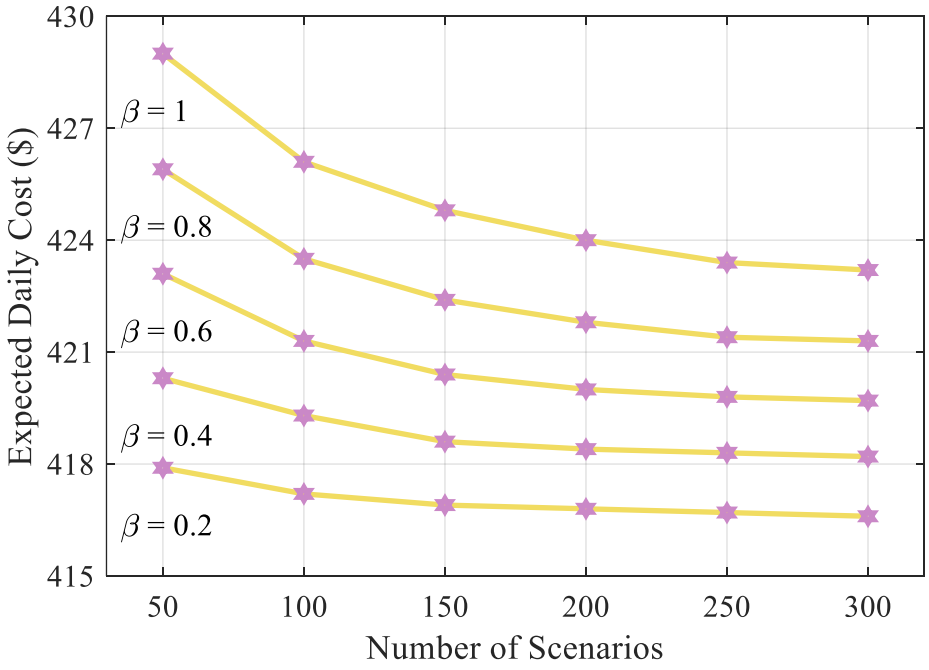

Figure 5-10: Operating Cost Comparison with Different Number of Scenarios.

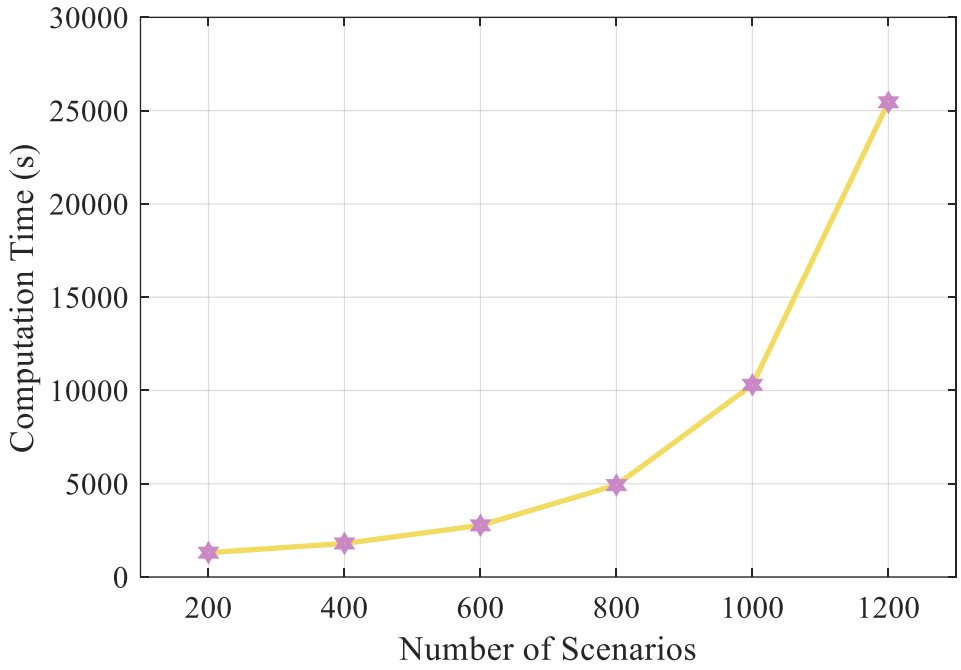

Figure 5-11: Computation Time with Different Number of Scenarios.

5.6. Case VI: Comparative Studies of Various Forecasting Methods

In Case VI, the proposed methods with different forecasting method are compared with other typical MES optimal scheduling methods in the literature, including dynamic programming in [10], MILP-based integrated optimization method in [14], and heuristic genetic-algorithm-based method in [29], in terms of operating cost and computation time. Same with the setting in Case II, the recorded actual data of each day in December 2019 is adopted for operation optimization, β and

initial stored energy in BS and HS are set to 0.

Table 5-2 first shows the average expected daily operating cost based on these methods. From the results, it can be seen that the operating costs of methods #1 to #5 that adopting forecast updating function are less than that of methods #6 to #9 that without such function. This is consistent with the results in Case III. By quickly and constantly incorporating the latest information of future demands and solar power, the previous forecasting deviations can be better corrected, and the storages can be better scheduled for the remaining horizon, therefore, the operating cost can be improved.

Among those methods with forecast updating, by comparing methods #1 and #5, we can see the two-stage scheduling method can generate close operating cost with the integrated method but with much shorter computation time. This is because in the second-stage optimization of the two-stage method, many variables that have been calculated in the first-stage optimization are fixed, thus the method can greatly reduce the computation burden and shorten the computation time.

Besides, comparing among methods #1 to #4, we see the method #1 with adaptive RF forecasting method outperform others when it comes to operating cost. This is because the adaptive RF can adjust to the latest forecasting condition so as improving the forecasting accuracy.

Table 5-2 also lists the average daily computation time for each method. This part of the simulation was run compared in an Intel Processor 5Y70 CPU 1.3 GHz environment. We see the computation times of method #1 and #2 may worse than that of methods #3 and #4. This is because RF models are generally complicated than ANN and ARMA models regard structure.

Besides, if the forecast updating feature is removed from the proposed two-stage method by setting the forecasting interval to 24 hours as marked with method #6 in the Table, its computation time is still much less than that of benchmark methods #7 to #9. While the generated operating cost would be higher than that of the integrated methods in [10] and [14] but still lower than that of the

genetic-algorithm-based method in [29].

Generally, based on the feature of forecast updating and two-stage optimization structure, the proposed MES optimal scheduling method is superior to other typical methods in the literature in terms of operating cost and computation time.

Table 5-2: Comparison of different MES optimal scheduling methods.

#	Method	Cost ($)	Time (s)
1	Two-Stage Method with Forecast Updating and adaptive RF	415	160.9
2	Two-Stage Method with Forecast Updating and classic RF	418	151.2
3	Two-Stage Method with Forecast Updating and ANN	419	141.6
4	Two-Stage Method with Forecast Updating and ARMA	443	138.2
5	Integrated Method with Forecast Updating and adaptive RF	413	523.2
6	Two-Stage Method without Forecast Updating	517	128.6
7	Dynamic Programming [10]	512	583.3
8	Mixed Integer Linear Programming [14]	510	497.7
9	Genetic Algorithm [29]	521	822.5

As a summary, this chapter first demonstrated the two reasons for selecting RF as the forecasting model through simulation results: One is that RF can provide forecasting result distribution, so that subsequent optimization can consider a variety of possible future scenarios. The second is the online updating function based on RF, which can achieve more accurate prediction results than other prediction models, thereby helping to reduce the operating cost of MES. In addition, by comparing the calculation time with other methods, we can also see the advantages of the proposed two-stage method in terms of calculation speed.

Chapter 6

Summary, Conclusions, and Future Work

In this thesis, different optimal scheduling methods of a real MES with hydrogen-based vehicle applications are studied from an economic point of view. The main contribution of this work is fourfold:

1) The previous scheduling methods usually neglecting the forecasting part. However, the designed optimization should be combined with the characteristics of the forecasting. Therefore, it is difficult for users to find a matching forecasting method. In this work, Random Forest forecasting model is applied and modified to provide inputs for the optimization considering multiple possible scenarios in the future. The entire scheduling method is more systematic.

2) A new two-stage optimization is proposed, which can greatly reduce computation time. Thus, the scheduling of MES operation can be conducted in much shorter time interval while considering more possible future scenarios.

3) In addition to the battery storage system as in other MESs in the literature, this work also considers the FCEV's hydrogen storage system and charging station. The existence of HS can further improve the operational flexibility within the scheduling horizon.

4) Based on the real MES data from Stone Edge Farm, the proposed optimization scheduling method is analyzed and simulated, and the real characteristics of MES devices are studied.

As the simulation results suggest, the proposed two-stage optimal scheduling method can help quantify the daily operating cost, balance real-time power demands and solar power, and achieve considerably operating cost saving for the Stone Edge Farm MES.

As for future work, following four aspects are considered:

1) More practical device constraints are expected to be included, for examples, the startup and cooldown time of devices in MESs. When the devices in the MES are turned on, it is difficult for them to work immediately and output the power required by the system. So how to ensure that various demands can be satisfied at any time according to the startup time of different devices is what we need to consider. In addition, based on the characteristics of certain devices, once we have turn them off, they must enter a cooldown state for a certain period upon use, such as CHP. Thus, in the scheduling, we also need to consider the situation where a device is needed to work immediately after turning it off due to the uncertainties from demand.

2) A selling power function is expected to be included in the optimization model. In the current setting, the BS can only store the solar energy according to the system demand on that day, and if there was such a selling power function of the optimization model that it can sell electricity back to the grid, the BS can store more solar energy and therefore the MES can make extra profit through selling power. This economic benefit will be even greater in the summer. Currently we are using winter data to do the simulation, but in summer, the system will have more solar power, and this selling power function will also generate more benefits.

3) In the current forecasting and optimization model, we assume that electricity prices and natural gas prices are given, because this is the case for our Stone Edge Farm. But other MESs may not have such a given price, so we need to predict energy prices and analyze their impact on system operating costs. On the one hand, we will need to modify the corresponding forecasting models since the volatility of energy prices in the real-time market is much higher than that of

energy demand. On the other hand, if electricity prices are taken into consideration, we are also considering adding some demand response functions.

4) We are also considering making a MATLAB SIMULINK block for each main device in MES. The constraints in the current optimization setting are all based on Stone Edge Farm MES. But if it is another MES, the number of various devices is different, and the network of various energy carriers in the system is also different. In this case, the users need to modify the constraints in the optimization when applying the method, especially the power flow balance equations, which causes inconvenience in use. But if each major device has a corresponding SIMULINK block, the users can easily describe the MES they are using by modifying the number of blocks and the corresponding connections, to easily realize optimization for the system operation. Previously we have done block modeling of the main devices in Microgrid for ABB, and the results have proved that this manner is indeed convenient for the users.

Bibliography

[1] Pan Z, Guo Q, Sun H. Feasible region method based integrated heat and electricity dispatch considering building thermal inertia. Applied Energy. 2017 Apr 15;192:395-407.

[2] Xu X, Jin X, Jia H, Yu X, Li K. Hierarchical management for integrated community energy systems. Applied Energy. 2015 Dec 15;160:231-43.

[3] Hemmes K, Zachariah-Wolf JL, Geidl M, Andersson G. Towards multi-source multi-product energy systems. International Journal of Hydrogen Energy. 2007 Jul 1;32(10-11):1332-8.

[4] Frik R, Favre-Perrod P. Proposal for a multifunctional energy bus and its interlink with generation and consumption. High voltage Laboratory, ETH, Zurich. 2004.

[5] Geidl M, Andersson G. Optimal power flow of multiple energy carriers. IEEE Transactions on power systems. 2007 Jan 29;22(1):145-55.

[6] Li G, Zhang R, Jiang T, Chen H, Bai L, Li X. Security-constrained bi-level economic dispatch model for integrated natural gas and electricity systems considering wind power and power-to-gas process. Applied energy. 2017 May 15;194:696-704.

[7] Quelhas A, Gil E, McCalley JD, Ryan SM. A multiperiod generalized network flow model of the US integrated energy system: Part I—Model description. IEEE transactions on power systems. 2007 Apr 30;22(2):829-36.

[8] Meibom P, Hilger KB, Madsen H, Vinther D. Energy comes together in Denmark: The key to a future fossil-free Danish power system. IEEE power and energy magazine. 2013 Aug 15;11(5):46-55.

[9] Guidelines on the development of “Internet+” Smart Energy (Energy Internet) [EB/OL].http://www.sdpc.gov.cn/zcfb/zcfbtz/201602/t20160229_790900.html (in Chinese).

[10] Moazeni S, Miragha AH, Defourny B. A risk-averse stochastic dynamic programming approach to energy hub optimal dispatch. IEEE Transactions on Power Systems. 2018 Nov 21;34(3):2169-78.

[11] Martelli E, Freschini M, Zatti M. Optimization of renewable energy subsidy and carbon tax for multi energy systems using bilevel programming. Applied Energy. 2020 Jun 1;267:115089.

[12] Chen C, Sun H, Shen X, Guo Y, Guo Q, Xia T. Two-stage robust planning-operation co-optimization of energy hub considering precise energy storage economic model. Applied Energy. 2019 Oct 15;252:113372.

[13] Wang Y, Zhang N, Zhuo Z, Kang C, Kirschen D. Mixed-integer linear programming-based optimal configuration planning for energy hub: Starting from scratch. Applied energy. 2018 Jan 15;210:1141-50.

[14] Moser A, Muschick D, Gölles M, Nageler P, Schranzhofer H, Mach T, Tugores CR, Leusbrock I, Stark S, Lackner F, Hofer A. A MILP-based modular energy management system for urban multi-energy systems: Performance and sensitivity analysis. Applied Energy. 2020 Mar 1;261:114342.

[15] Mei J, Wang X, Kirtley JL. Optimal scheduling of real multi-carrier energy storage system with hydrogen‐based vehicle applications. IET Renewable Power Generation. 2020 Feb;14(3):381-8.

[16] Qiu J, Dong ZY, Zhao JH, Meng K, Zheng Y, Hill DJ. Low carbon oriented expansion planning of integrated gas and power systems. IEEE Transactions on Power Systems. 2014 Dec 10;30(2):1035-46.

[17] Schulze M, Del Granado PC. Optimization modeling in energy storage applied to a multi-carrier system. InIEEE PES General Meeting 2010 Jul 25 (pp. 1-7). IEEE.

[18] Najafi A, Falaghi H, Contreras J, Ramezani M. A stochastic bilevel model for the energy hub manager problem. IEEE Transactions on Smart Grid. 2016 Oct 19;8(5):2394-404.

[19] Jiang Y, Wan C, Chen C, Shahidehpour M, Song Y. A hybrid stochastic-interval operation strategy for multi-energy microgrids. IEEE Transactions on Smart Grid. 2019 Jun 20;11(1):440-56.

[20] Li P, Wang Z, Wang J, Yang W, Guo T, Yin Y. Two-stage optimal operation of integrated energy system considering multiple uncertainties and integrated demand response. Energy. 2021 Jun 15;225:120256.

[21] Mirzaei MA, Yazdankhah AS, Mohammadi-Ivatloo B, Marzband M, Shafie-khah M, Catalão JP. Stochastic network-constrained co-optimization of energy and reserve products in renewable energy integrated power and gas networks with energy storage system. Journal of cleaner production. 2019 Jun 20;223:747-58.

[22] Shahrabi E, Hakimi SM, Hasankhani A, Derakhshan G, Abdi B. Developing optimal energy management of energy hub in the presence of stochastic renewable energy resources. Sustainable Energy, Grids and Networks. 2021 Jun 1;26:100428.

[23] Heidari A, Mortazavi SS, Bansal RC. Stochastic effects of ice storage on improvement of an energy hub optimal operation including demand response and renewable energies. Applied Energy. 2020 Mar 1;261:114393.

[24] Zhao T, Pan X, Yao S, Ju C, Li L. Strategic bidding of hybrid AC/DC microgrid embedded energy hubs: A two-stage chance constrained stochastic programming approach. IEEE Transactions on Sustainable Energy. 2018 Dec 4;11(1):116-25.

[25] Liu J, Xu Z, Wu J, Liu K, Guan X. Optimal planning of distributed hydrogen-based multi-energy systems. Applied Energy. 2021 Jan;281:116107.

[26] Lei Y, Wang D, Jia H, Chen J, Li J, Song Y, Li J. Multi-objective stochastic expansion planning based on multi-dimensional correlation scenario generation method for regional integrated energy system integrated renewable energy. Applied Energy. 2020 Oct 15;276:115395.

[27] Wu L, Shahidehpour M. Optimal coordination of stochastic hydro and natural gas supplies in midterm operation of power systems. IET generation, transmission & distribution. 2011 May 1;5(5):577-87.

[28] Mayer MJ, Szilágyi A, Gróf G. Environmental and economic multi-objective optimization of a household level hybrid renewable energy system by genetic algorithm. Applied Energy. 2020 Jul 1;269:115058.

[29] Kampouropoulos K, Andrade F, Sala E, Espinosa AG, Romeral L. Multiobjective optimization of multi-carrier energy system using a combination of ANFIS and genetic algorithms. IEEE Transactions on Smart Grid. 2016 Sep 14;9(3):2276-83.

[30] Moeini-Aghtaie M, Abbaspour A, Fotuhi-Firuzabad M, Hajipour E. A decomposed solution to multiple-energy carriers optimal power flow. IEEE Transactions on Power Systems. 2013 Oct 9;29(2):707-16.

[31] Cao Y, Wei W, Wang J, Mei S, Shafie-khah M, Catalao JP. Capacity planning of energy hub in multi-carrier energy networks: A data-driven robust stochastic programming approach. IEEE Transactions on Sustainable Energy. 2018 Oct 26;11(1):3-14.

[32] Zhang Y, Liu Y, Shu S, Zheng F, Huang Z. A data-driven distributionally robust optimization model for multi-energy coupled system considering the temporal-spatial correlation and distribution uncertainty of renewable energy sources. Energy. 2021 Feb 1;216:119171.

[33] Ali U, Shamsi MH, Bohacek M, Purcell K, Hoare C, Mangina E, O'Donnell J. A data-driven approach for multi-scale GIS-based building energy modeling for analysis, planning and support decision making. Applied Energy. 2020 Dec 1;279:115834.

[34] Bahrami S, Sheikhi A. From demand response in smart grid toward integrated demand response in smart energy hub. IEEE Transactions on Smart Grid. 2015 Aug 17;7(2):650-8.

[35] Alipour M, Zare K, Abapour M. MINLP probabilistic scheduling model for demand response programs integrated energy hubs. IEEE Transactions on Industrial Informatics. 2017 Jul 21;14(1):79-88.

[36] Pazouki S, Haghifam MR. Optimal planning and scheduling of energy hub in presence of wind, storage and demand response under uncertainty. International Journal of Electrical Power & Energy Systems. 2016 Sep 1;80:219-39.

[37] Li X, Zhang R, Bai L, Li G, Jiang T, Chen H. Stochastic low-carbon scheduling with carbon capture power plants and coupon-based demand response. Applied energy. 2018 Jan 15;210:1219-28.

[38] Xu W, Zhou D, Huang X, Lou B, Liu D. Optimal allocation of power supply systems in industrial parks considering multi-energy complementarity and demand response. Applied Energy. 2020 Oct 1;275:115407.

[39] Su Y, Zhou Y, Tan M. An interval optimization strategy of household multi-energy system considering tolerance degree and integrated demand response. Applied Energy. 2020 Feb 15;260:114144.

[40] Zheng S, Sun Y, Li B, Qi B, Zhang X, Li F. Incentive-based integrated demand response for multiple energy carriers under complex uncertainties and double coupling effects. Applied Energy. 2021 Feb 1;283:116254.

[41] Bai L, Li F, Cui H, Jiang T, Sun H, Zhu J. Interval optimization based operating strategy for gas-electricity integrated energy systems considering demand response and wind uncertainty. Applied energy. 2016 Apr 1;167:270-9.

[42] Carmo M, Fritz DL, Mergel J, Stolten D. A comprehensive review on PEM water electrolysis. International journal of hydrogen energy. 2013 Apr 22;38(12):4901-34.

[43] Joshi AS, Dincer I, Reddy BV. Exergetic assessment of solar hydrogen production methods. International Journal of Hydrogen Energy. 2010 May 1;35(10):4901-8.

[44] Sui J, Chen Z, Wang C, Wang Y, Liu J, Li W. Efficient hydrogen production from solar energy and fossil fuel via water-electrolysis and methane-steam-reforming hybridization. Applied Energy. 2020 Oct 15;276:115409.

[45] Mikovits C, Wetterlund E, Wehrle S, Baumgartner J, Schmidt J. Stronger together: Multi-annual variability of hydrogen production supported by wind power in Sweden. Applied Energy. 2021 Jan 15;282:116082.

[46] Steinfeld A. Solar hydrogen production via a two-step water-splitting thermochemical cycle based on Zn/ZnO redox reactions. International journal of hydrogen energy. 2002 Jun 1;27(6):611-9.

[47] Liu J, Xu Z, Wu J, Liu K, Guan X. Optimal planning of distributed hydrogen-based multi-energy systems. Applied Energy. 2021 Jan;281:116107.

[48] Mansour-Saatloo A, Agabalaye-Rahvar M, Mirzaei MA, Mohammadi-Ivatloo B, Abapour M, Zare K. Robust scheduling of hydrogen based smart micro energy hub with integrated demand response. Journal of Cleaner Production. 2020 Sep 10;267:122041.

[49] AlRafea K, Fowler M, Elkamel A, Hajimiragha A. Integration of renewable energy sources into combined cycle power plants through electrolysis generated hydrogen in a new designed energy hub. International journal of hydrogen energy. 2016 Oct 15;41(38):16718-28.

[50] Peng DD, Fowler M, Elkamel A, Almansoori A, Walker SB. Enabling utility-scale electrical energy storage by a power-to-gas energy hub and underground storage of hydrogen and natural gas. Journal of Natural Gas Science and Engineering. 2016 Sep 1;35:1180-99.

[51] Stone Edge Farm. https://sefmicrogrid.com/resources/gallery/

[52] Liu X, Wu J, Jenkins N, Bagdanavicius A. Combined analysis of electricity and heat networks. Applied Energy. 2016 Jan 15;162:1238-50.

[53] Geidl M, Koeppel G, Favre-Perrod P, Klockl B, Andersson G, Frohlich K. Energy hubs for the future. IEEE power and energy magazine. 2006 Dec 26;5(1):24-30.

[54] Capstone Gas Turbine C65. https://www.pureworldenergy.com/technology/capstone-products/c65-capstone-microturbine/

[55] Electric Heap Pump System. https://www.entekhvac.com/pros-and-cons-of-an-electric-heat-pump/

[56] Tesla Lithium-ion batteries. https://www.tesla.com/powerpack

[57] Millennium Reign Energy. https://residentialhydrogenpower.com/

[58] Mei J, He D, Harley R, Habetler T, Qu G. A random forest method for real-time price forecasting in New York electricity market. In2014 IEEE PES General Meeting| Conference & Exposition 2014 Jul 27 (pp. 1-5). IEEE.

[59] Breiman L. Random forests. Machine learning. 2001 Oct;45(1):5-32.

[60] Chrysos G, Dagritzikos P, Papaefstathiou I, Dollas A. HC-CART: A parallel system implementation of data mining classification and regression tree (CART) algorithm on a multi-FPGA system. ACM Transactions on Architecture and Code Optimization (TACO). 2013 Jan 20;9(4):1-25.

[61] Rodriguez-Galiano VF, Ghimire B, Rogan J, Chica-Olmo M, Rigol-Sanchez JP. An assessment of the effectiveness of a random forest classifier for land-cover classification. ISPRS Journal of Photogrammetry and Remote Sensing. 2012 Jan 1;67:93-104.

[62] Talukdar S, Eibek KU, Akhter S, Ziaul S, Islam AR, Mallick J. Modeling fragmentation probability of land-use and land-cover using the bagging, random forest and random subspace in the Teesta River Basin, Bangladesh. Ecological Indicators. 2021 Jul 1;126:107612.

[63] Shim EJ, Yoon MA, Yoo HJ, Chee CG, Lee MH, Lee SH, Chung HW, Shin MJ. An MRI-based decision tree to distinguish lipomas and lipoma variants from well-differentiated liposarcoma of the extremity and superficial trunk: Classification and regression tree (CART) analysis. European journal of radiology. 2020 Jun 1;127:109012.

[64] Ho TK. The random subspace method for constructing decision forests. IEEE transactions on pattern analysis and machine intelligence. 1998 Aug;20(8):832-44.

[65] Zhu M, Xia J, Jin X, Yan M, Cai G, Yan J, Ning G. Class weights random forest algorithm for processing class imbalanced medical data. IEEE Access. 2018 Jan 4;6:4641-52.

[66] Alam MZ, Rahman MS, Rahman MS. A Random Forest based predictor for medical data classification using feature ranking. Informatics in Medicine Unlocked. 2019 Jan 1;15:100180.

[67] Wei S, Zhou X, Wu W, Pu Q, Wang Q, Yang X. Medical image super-resolution by using multi-dictionary and random forest. Sustainable Cities and Society. 2018 Feb 1;37:358-70.

[68] Lei Y, Wang T, Harms J, Shafai-Erfani G, Tian S, Higgins K, Shu HK, Shim H, Mao H, Curran WJ, Liu T. MRI-based pseudo CT generation using classification and regression random forest. InMedical Imaging 2019: Physics of Medical Imaging 2019 Mar 1 (Vol. 10948, p. 1094843). International Society for Optics and Photonics.

[69] CUI J, MIAO J, CHEN J. Research on the Impetus of China's Economic Growth Based on Random Forest. Research on Economics and Management. 2015:03.

[70] Gounaridis D, Chorianopoulos I, Symeonakis E, Koukoulas S. A Random Forest-Cellular Automata modelling approach to explore future land use/cover change in Attica (Greece), under different socio-economic realities and scales. Science of the Total Environment. 2019 Jan 1;646:320-35.

[71] Sherafatpour Z, Roozbahani A, Hasani Y. Agricultural water allocation by integration of hydro-economic modeling with Bayesian networks and random forest approaches. Water Resources Management. 2019 May;33(7):2277-99.

[72] Oliveira S, Oehler F, San-Miguel-Ayanz J, Camia A, Pereira JM. Modeling spatial patterns of fire occurrence in Mediterranean Europe using Multiple Regression and Random Forest. Forest Ecology and Management. 2012 Jul 1;275:117-29.

[73] Xu R, Luo F. Risk prediction and early warning for air traffic controllers' unsafe acts using association rule mining and random forest. Safety science. 2021 Mar 1;135:105125.

[74] Shang Q, Tan D, Gao S, Feng L. A hybrid method for traffic incident duration prediction using BOA-optimized random forest combined with neighborhood components analysis. Journal of Advanced Transportation. 2019 Jan 20;2019.

[75] Krishnaveni S, Hemalatha M. A perspective analysis of traffic accident using data mining techniques. International Journal of Computer Applications. 2011 Jun 7;23(7):40-8.

[76] Yoo C, Han D, Im J, Bechtel B. Comparison between convolutional neural networks and random forest for local climate zone classification in mega urban areas using Landsat images. ISPRS Journal of Photogrammetry and Remote Sensing. 2019 Nov 1;157:155-70.

[77] Hashimoto H, Wang W, Melton FS, Moreno AL, Ganguly S, Michaelis AR, Nemani RR. High‐resolution mapping of daily climate variables by aggregating multiple spatial data sets with the random forest algorithm over

the conterminous United States. International Journal of Climatology. 2019 May;39(6):2964-83.

[78] Gaál M, Moriondo M, Bindi M. Modelling the impact of climate change on the Hungarian wine regions using random forest. Appl. Ecol. Environ. Res. 2012 May;10(2):121-40.

[79] Tomin N, Zhukov A, Sidorov D, Kurbatsky V, Panasetsky D, Spiryaev V. Random forest based model for preventing large-scale emergencies in power systems. International Journal of Artificial Intelligence. 2015 Oct;13(1):211-28.

[80] Liu D, Sun K. Random forest solar power forecast based on classification optimization. Energy. 2019 Nov 15;187:115940.

[81] Sekhar P, Mohanty S. Classification and assessment of power system static security using decision tree and random forest classifiers. International Journal of Numerical Modelling: Electronic Networks, Devices and Fields. 2016 May;29(3):465-74.

[82] Lahouar A, Slama JB. Day-ahead load forecast using random forest and expert input selection. Energy Conversion and Management. 2015 Oct 1;103:1040-51.

[83] Saffari A, Leistner C, Santner J, Godec M, Bischof H. On-line random forests. In2009 ieee 12th international conference on computer vision workshops, iccv workshops 2009 Sep 27 (pp. 1393-1400). IEEE.

[84] Hastie T, Tibshirani R, Friedman J. The Elements of Statistical Learning: Prediction. Inference and Data Mining: Springer Verlag. 2009.

[85] Akhoondzadeh M. Decision Tree, Bagging and Random Forest methods detect TEC seismo-ionospheric anomalies around the time of the Chile,(Mw= 8.8) earthquake of 27 February 2010. Advances in Space Research. 2016 Jun 15;57(12):2464-9.

[86] Toloşi L, Lengauer T. Classification with correlated features: unreliability of feature ranking and solutions. Bioinformatics. 2011 Jul 15;27(14):1986-94.

[87] Jiang P, Li R, Liu N, Gao Y. A novel composite electricity demand forecasting framework by data processing and optimized support vector machine. Applied Energy. 2020 Feb 15;260:114243.

[88] Wen L, Zhou K, Yang S. Load demand forecasting of residential buildings using a deep learning model. Electric Power Systems Research. 2020 Feb 1;179:106073.

[89] Zhang G, Guo J. A novel method for hourly electricity demand forecasting. IEEE Transactions on Power Systems. 2019 Sep 16;35(2):1351-63.

[90] Heydari A, Garcia DA, Keynia F, Bisegna F, De Santoli L. A novel composite neural network based method for wind and solar power forecasting in microgrids. Applied Energy. 2019 Oct 1;251:113353.

[91] Ahmed R, Sreeram V, Mishra Y, Arif MD. A review and evaluation of the state-of-the-art in PV solar power forecasting: Techniques and optimization. Renewable and Sustainable Energy Reviews. 2020 May 1;124:109792.

[92] Mandal P, Srivastava AK, Negnevitsky M, Park JW. An effort to optimize similar days parameters for ANN based electricity price forecasting. In2008 IEEE Industry Applications Society Annual Meeting 2008 Oct 5 (pp. 1-9). IEEE.

[93] Ghode T, Begum KM, Desamala AB, Narayanan A. A comparative study of ANN and CFD modelling for pressure drop prediction in a fluidized bed with internals. Indian Chemical Engineer. 2017 Jan 2;59(1):57-75.

[94] Kaiser R, Kim S, Lee D. Deep data analysis for aspiration pressure estimation in a high-pressure gas atomization process using an artificial neural network. Chemical Engineering and Processing-Process Intensification. 2020 Jul 1;153:107924.

[95] Scholz M, Fraunholz M, Selbig J. Nonlinear principal component analysis: neural network models and applications. InPrincipal manifolds for data visualization and dimension reduction 2008 (pp. 44-67). Springer, Berlin, Heidelberg.

[96] Whittle P. On stationary processes in the plane. Biometrika. 1954 Dec 1:434-49.

[97] Whittle P. Estimation and information in stationary time series. Arkiv för matematik. 1953 Aug;2(5):423-34.

[98] Pappas SS, Ekonomou L, Karamousantas DC, Chatzarakis GE, Katsikas SK, Liatsis P. Electricity demand loads modeling using AutoRegressive Moving Average (ARMA) models. Energy. 2008 Sep 1;33(9):1353-60.

[99] Valipour M, Banihabib ME, Behbahani SM. Parameters estimate of autoregressive moving average and autoregressive integrated moving average models and compare their ability for inflow forecasting. J Math Stat. 2012;8(3):330-8.

[100] Pham HT, Yang BS. A hybrid of nonlinear autoregressive model with exogenous input and autoregressive moving average model for long-term machine state forecasting. Expert Systems with Applications. 2010 Apr 1;37(4):3310-7.

[101] Liu L, Ding F, Xu L, Pan J, Alsaedi A, Hayat T. Maximum likelihood recursive identification for the multivariate equation-error autoregressive moving average systems using the data filtering. IEEE Access. 2019 Mar 18;7:41154-63.

[102] Li M, Liu X, Ding F. The filtering‐based maximum likelihood iterative estimation algorithms for a special class of nonlinear systems with autoregressive moving average noise using the hierarchical identification principle. International Journal of Adaptive Control and Signal Processing. 2019 Jul;33(7):1189-211.

[103] Mei J, Zuo Y, Lee CH, Wang X, Kirtley JL. Stochastic optimization of multi-energy system operation considering hydrogen-based vehicle applications. Advances in Applied Energy. 2021 May 26;2:100031.